Thermodynamic Gradient-based Poroplastic Theory for Concrete under High Temperatures

Marianela Ripani, Guillermo Etse, Sonia Vrech, Javier Mroginski

PII: S0749-6419(14)00116-8
DOI: http://dx.doi.org/10.1016/j.ijplas.2014.06.001
Reference: INTPLA 1800

To appear in: *International Journal of Plasticity*

Received Date: 16 February 2014
Revised Date: 6 June 2014

Please cite this article as: Ripani, M., Etse, G., Vrech, S., Mroginski, J., Thermodynamic Gradient-based Poroplastic Theory for Concrete under High Temperatures, *International Journal of Plasticity* (2014), doi: http://dx.doi.org/10.1016/j.ijplas.2014.06.001

Thermodynamic Gradient-based Poroplastic Theory for Concrete under High Temperatures

Marianela Ripani[a], Guillermo Etse[a], Sonia Vrech[b], Javier Mroginski[b]

[a] *CONICET-National Scientific and Technical Research Council, Materials and Structures Laboratory, University of Buenos Aires, Argentina.*
[b] *CONICET, Center for Numerical and Computational Methods in Engineering, National University of Tucumán, Argentina*

Abstract

Concrete materials subjected to long term exposures to high temperatures suffer severe degradations in its mechanical properties (cohesion, friction, strength and stiffness) and changes in their failure mechanisms. These degradations may lead to irreversible damage or sudden collapse of the related structures. From the predictive analysis stand point, accurate constitutive theories are required to simulate the variations of concrete mechanical failure behavior under high and durable temperature fields. In the realm of the smeared crack approach, non-local model strategies are required to objectively reproduce failure behaviors under coupled thermo-mechanical loading conditions, while realistic descriptions of the involved characteristic lengths are needed to objectively reproduce the variation from ductile to brittle failure modes depending on the acting confining pressure and temperature. In this work, a thermodynamically consistent gradient poroplastic model for concrete subjected to high temperatures is proposed. A particular and simple form of gradient-based poroplasticity is considered whereby the state variables are the only ones of non-local character. The degradations of these variables due to coupled thermo-mechanical effects are described in the framework of the thermodynamic approach. After describing the material formulation, numerical analyses are presented which demonstrate the predictive capabilities of the proposed constitutive theory for different stress paths and thermal conditions.

Keywords: Concrete, Gradient Theory, Thermodynamic Consistency, High Temperature, Failure Behavior

1. Introduction

When concrete structures are subjected to high temperatures in long term exposures, two effects turn evident. On the one hand, and as a result of the dehydration process of the cement paste, there is an irreversible degradation of two fundamental material properties: the elastic stiffness (thermal damage) and the material strength (thermal decohesion). On the other hand, a particular failure or fracture mode develops, the so-called concrete spalling, characterized by fracture planes parallel to the heated surface and perpendicular to the temperature flux. The spalling effect on heated concrete is due to the pressure buildup in the pores. A clear explanation of the mechanism that causes concrete spalling was provided by Ulm and Coussy (1999). They pointed out that concrete heating rapidly leads to the formation of a moisture clog in the vicinity of the heated surface. Consequently, high pressures are induced in these zones due to the low concrete permeability and, therefore, concrete spalling develops.

Temperature effects on concrete vary with the temperature level. At temperatures below 200°C, only the expelling of water vapor through the network of connected concrete pores takes place. Consequently, up to 200°C no significant change in concrete mechanical properties is evidenced (Mihashi et al., 1992), while the limited concrete damage is mainly due to temperature gradients. The dehydration of calcium silicate hydrate (CSH) starts at temperatures above 200°C. On the other hand, calcium hydroxide ($Ca(OH)_2$) starts to chemically breakdown at 500°C, while CSH does this at 700°C. Above 500°C, the chemical and mechanical changes become substantial and irreversible. It can be concluded that, when concrete is subjected to a temperature field above the 200°C threshold in long term exposure, the degradation of its cohesive properties due to the cement paste dehydration turns out to be the most relevant consequence.

This effect strongly influences the mechanical behavior and the overall strength capacity of the related structures. Regarding the influence of the concrete performance on its sensitivity to high temperatures, many authors agree that

high strength concretes turn more brittle when they are subjected to high temperatures, see among others Chan et al. (1996, 1999); Balendran et al. (2003); Gawin et al. (2004); Li et al. (2004); Mehmet and Ozturan (2010) and Zhen-jun and Yu-pu (2010).

From the theoretical and analytical stand points, many different attempts have been made to describe and predict the behavior of concrete under long term exposure to high temperatures. Most of them are related to local constitutive theories, while very few non-local formulations are thermodynamically consistent. Actually, many developments are related to the so-called hygrothermal models. They are able to predict the pore pressure and temperature gradient evolutions, but not the temperature effect on concrete mechanical properties and their degradation. Among others, we refer here to the works by Majumdar et al. (1995); Jooss and Reinhardt (2002); Feraille-Fresnet et al. (2003); Chung and Consolazio (2005) and Zeim et al. (2008). The proposal by Mindeguia et al. (2010) also takes into account chemically bound water diffusion while Tenchev et al. (2001, 2005) consider the coupling of a hygro-thermal model with the mechanical damage model by Ortiz (1985).

Most of the proposed constitutive theories for concrete under high temperature are related to classical non-porous media. In this framework, Khennane and Baker (1992a,b) formulated the variation of concrete mechanical properties with temperature, while Zhou et al. (1998) defined a consistent set of governing equations to model the coupled thermo-hygro-mechanical process in deformable unsaturated porous media. In the same framework, Gawin et al. (1998) proposed a constitutive model to analyze concrete heat and mass transfers at high temperatures and the resulting mechanical behavior including damage effects. This formulation was modified by Gawin et al. (2003) to take into account the coupled thermo-chemical concrete damage and further by Gawin et al. (2006) to account for the thermal spalling risk.

One of the first contributions related to the analysis of concrete under high temperatures in the porous media framework was made by Ulm and Coussy (1999). Their approach was based on the concept of chemoplastic softening due to cement paste dehydration caused by high temperatures. In this formulation, concrete is modeled as a chemically reactive porous medium with thermo-chemo-mechanical couplings. Actually, the dehydration model may be considered as the opposite case of the hydration one (Ulm and Coussy, 1995, 1996; Prato et al., 1997; Martinelli et al., 2013).

A similar proposal to that of Ulm and Coussy (1999) was presented by Sercombe et al. (1998) who developed a chemoplastic model based on a closest-point projection algorithm.

A thermo-hygro-chemical model based on porous media concepts was proposed by Dal Pont and Ehrlacher (2004) whereby non-linear phenomena, heat and mass transfers, and the evolution of the porous phase features are taken into account within a full coupled consideration. In this proposal, however, the solid skeleton is considered as rigid, which is a relevant limitation to accurately reproduce the non-linear behavior of concrete under high temperatures. Another shortcoming of this proposal, from the theoretical stand point, is the lack of a thermodynamic basis.

Canadija and Brnic (2004) proposed a J_2 thermoplasticity model accounting for finite strains, which is more appropriated for ductile materials like metals, instead of cohesive-frictional ones, like concrete.

More recently, Obeid et al. (2011) studied the effects of thermo-hygro-mechanical couplings in porous media through the mechanics of unsaturated porous media. Temperature effects in porous materials were also taken into account by Wippler et al. (2011), being its main contribution the numerical homogenization of the effective thermoelastic properties of the two-phase material. In this sense, Zhang et al. (2012) studied the effects of the local thermal imbalance on the pore pressure and on the thermal stresses, for fluid-saturated porous media subjected to transient thermal loads, modeled within the framework of the thermo-poroelasticity.

Regarding spalling effects, De Morais et al. (2010) performed numerical analysis with a finite element code where the heat gradients and the water vapor pressure inside concrete elements were determined by means of a thermo-hydrous model. In this case, the mechanical stresses were evaluated with an isotropic linear elastic law and an isotropic elastoplastic model. More recently, Pan et al. (2012) studied the effect of aggregate size on concrete spalling due to fire. They were able to demonstrate that the degree of spalling bears a good correlation to the length of the fracture process zone, and that this length increases with the aggregate size.

Most of the existing proposals for constitutive theories for concrete under high temperatures are related to local theories. As it is well known, the post-peak predictions of local or classical continuum models suffer from strong objectivity loss regarding mesh size and finite element orientations. This is due to the onset of discontinuous bifurcations which lead to the loss of strong ellipticity of the associated differential equations.

The first and simplest attempt to solve the deficiencies of local material formulations was the inclusion of fracture

energy concepts in the softening law, see Bazant and Oh (1983); Willam et al. (1984) and Etse and Willam (1994). Despite its effectiveness at regularizing the load-displacement behavior of smeared crack constitutive theories, fracture energy-based formulations are unable to solve the ill-possedness of the differential equations and, therefore, they lead to mesh-dependent solutions of the shear band width and deformed patterns. The micropolar Cosserat theory has been more effective at regularizing the solutions of smeared crack constitutive laws and at suppressing the loss of ellipticity of the related differential equations. This theory was pioneered by Muehlhaus and Vardoulakis (1987) and de Borst (1991) and further applied by Sluys and de Borst (1991); Etse et al. (1991); Dietsche et al. (1993) and Etse et al. (2003). Among all non-local approaches for smeared crack constitutive formulations, the gradient theory is the most extensively used, due to its efficiency at regularizing post-peak behaviors under every possible stress state. The inclusion of higher strain gradients in material models was originally proposed for the study of slip bands in metals (Aifantis, 1984, 1987; Coleman and Hodgdon, 1985). Then Belytschko and Lasry (1989) enunciated a one-dimensional constitutive law dependent on gradients whih Aifantis and Zbib (1988) included in the creep condition.

For the analysis of shear bands in granular materials, a gradient-based plasticity model was proposed by Vardoulakis and Aifantis (1991). A selective fracture energy and gradient-based thermodynamically consistent formulation was proposed by Vrech and Etse (2009) to avoid the intrinsic and spurious failure diffusion predictions of gradient constitutive theories and its shortcomings to accurately describe the failure modes of quasi-brittle materials, like concrete.

In recent years, the non-local concepts were successfully extended to describe the non-lineal behavior of porous materials, see La Ragione et al. (2008); Muraleetharan et al. (2009) and Kamrin (2010). Likewise, the consideration of microscopic aspects in the formulation of non-local constitutive theories for porous and granular materials are due to Nicot and Darve (2007); Yin et al. (2009); Zhu et al. (2010) and Xie et al. (2011). Other remarkable works related to this matter were performed by Bonelli et al. (2012); Jiang and Shao (2012); Shen et al. (2012); Tran et al. (2012); Shen et al. (2013) and Shojaei et al. (2014). Bonelli et al. (2012) took into account the effect of grain rotations in the description of macroscopic strains. Jiang and Shao (2012) presented a fast Fourier transformation-based micromechanical analysis to simulate the nonlinear behavior of porous geomaterials. Shen et al. (2012, 2013) proposed a two-step homogenization procedure for multiscale analysis of clayey rocks; while Tran et al. (2012) developed a micromechanics-based approach for periodic linear elastic composites exhibiting strain gradient effects at the macroscopic level. Finally, Shojaei et al. (2014), based on a previous work by Shojaei et al. (2013), developed a continuum damage mechanics based constitutive model to describe elastic, plastic and damage behavior of porous rocks.

Discontinuous bifurcation analyses in porous media were performed by Nicot et al. (2009, 2012) and Mroginski and Etse (2014). Also, an alternative expression for the effective stress tensor was included in Xie and Sha (2012) and Nicot et al. (2013).

A specific application of thermodynamically-consistent gradient poroplastic theory for thermo-mechanical problems in metals was performed by Forest and Aifantis (2010). Later, Voyiadjis and Faghihi (2012) investigated the coupling of thermal and mechanical responses of materials in small scales and fast transient process, in the framework of higher-order strain gradient plasticity with interfacial energy effect. In a recent proposal by Abu Al-Rub and Darabi (2012) a general thermodynamic-based framework is proposed for deriving coupled temperature-dependent and time-dependent constitutive theories based on viscoelasticity, viscoplasticity, and viscodamage. In this sense, Loeffel and Anand (2011) proposed a thermodynamically-consistent, chemo-thermo-mechanically coupled theory for bond-coat materials with oxygen diffusion. Regarding the thermodynamic basis, it is remarkable the work presented by Voyiadjis et al. (2011) who proposed an interesting thermodynamic consistent model that includes plasticity and damage for viscoplastic materials, in particular polymers, which was generalized and extended to anisotropic materials in further works (Voyiadjis et al., 2012b,a).

Regarding quasi-brittle, partially saturated porous materials like concrete and soils, Mroginski et al. (2011), proposed a thermodynamically consistent gradient formulation, based on the original concept by Vrech and Etse (2009). In this work, a thermodynamically consistent gradient poroplastic theory is proposed for concrete under high temperatures effects.

The constitutive theory presented in this work is an extension of the formulation by Mroginski et al. (2011), which considers a restricted form of gradient plasticity, since the state variables are the only ones of non-local character. This new formulation accounts for temperature effects and for the related thermo-mechanical coupling of concrete materials when subjected to high temperatures. The model includes an isotropic and local hardening formulation that turns non-local in the softening regime, when a combined fracture energy and gradient-based description of the

strength degradation (as proposed by Vrech and Etse (2009)) is activated. To account for the thermal degradation, and following Coussy (1995), frozen entropy is incorporated, which describes the thermo-mechanic softening behavior. The model includes two characteristic lengths. One of them is related to the fracture energy released in the active cracks during coupled thermo-mechanical processes. The second characteristic length is related to the gradient-based formulation, and defines the zone width where thermo-mechanical degradation of the material located in between active cracks takes place. To realistically reproduce the strong dependence of concrete failure modes with the acting confining pressure, the temperature and the initial porosity, both characteristic lengths are defined in terms of these variables.

After presenting the constitutive theory and its formulation, the attention focuses on the numerical predictions of the proposed material model when it is subjected to uniaxial and triaxial compression regimes under different temperature levels. The results demonstrate the capabilities of the proposed constitutive theory to reproduce failure mechanisms of concrete under high temperatures and their variations with the acting confinement.

2. Porous media description

In order to describe the deformation and movement of a porous medium as a whole, the tools traditionally used for continuous media are applied, having also in mind the existence of a deformable skeleton and fluids in the porous space. In other words, it is taken into account the superimposition of two continua in time and space: skeleton and fluids. In the skeleton, the fluid mass exchange may take place only in the connected space.

It is worth distinguishing the matrix from the skeleton in its constitution and scale: the matrix is the solid material part of the skeleton. In other words, the matrix corresponds to a microscopic scale of description, whereas the skeleton refers to a macroscopic or, even, mesoscopic one. The porosity is referred to the representative elementary volume, which includes sufficient material to represent the macroscopic phenomenon studied therein.

The matrix may be composed of both a solid part and a disconnected occluded porous space. The total porosity of a given volume is the ratio of the fluid volume to the total volume. In this work the term porosity refers exclusively to the fluid located in the connected porosity.

Regarding the poroplastic theory, permanent strains not only take place in the skeleton, but also in the fluid mass content due to porosity variations either by mechanical o chemical effects. The chemical dehydration reaction is the passage of the water mass combined with the solid skeleton, to the fluid mass in the connected pore system.

3. Thermodynamic of Porous Media

3.1. First Law of Thermodynamics

The First Law of Thermodynamics is expressed in Eq.(1), which represents the balance equation between internal energy rate $\dot{E}$, kinetic energy rate $\dot{K}$, mechanic work of external forces P and externally supplied heat Q, see Coussy (1995). Hereinafter, the notation $\dot{(\,)}$ implies the temporal derivative of $(\,)$,

$$\dot{E} + \dot{K} = P + Q \tag{1}$$

with

$$\dot{E} = \frac{\mathrm{d}}{\mathrm{d}t}\int_{\Omega} e \,\mathrm{d}\Omega \tag{2}$$

$$\dot{K} = \frac{1}{2}\int_{\Omega}\left[\rho_s\,(1-\phi)\,\dot{\mathbf{u}}_s\cdot\dot{\mathbf{u}}_s + \rho_f\phi\,\mathbf{w}\cdot\mathbf{w}\right]\mathrm{d}\Omega \tag{3}$$

$$P = \int_{\partial\Omega}\left(\boldsymbol{\sigma}\cdot\mathbf{n}\cdot\dot{\mathbf{u}}_s - \frac{p}{\rho_f}\mathbf{n}\cdot\mathbf{w}\right)\mathrm{d}\partial\Omega + \int_{\Omega}\rho\,\mathbf{b}\cdot\dot{\mathbf{u}}_s\,\mathrm{d}\Omega \tag{4}$$

$$Q = \int_{\Omega}\rho r\,\mathrm{d}\Omega - \int_{\partial\Omega}\mathbf{h}\cdot\mathbf{n}\,\mathrm{d}\partial\Omega \tag{5}$$

being e the internal energy density, which results from the sum of e_s and e_f, where the subscripts s and f denote the skeleton and fluid components respectively. Moreover, $\mathbf{w}$ is the relative flow vector respect to the solid matrix, $\rho = \rho_s(1-\phi) + \rho_f\phi$ is the total density of the body, and ϕ is the porosity. Finally, $\mathbf{u}_s$ is the velocity vector of the skeleton.

Regarding the other terms, $\boldsymbol{\sigma}$ is the total Cauchy tensor, $\mathbf{b}$ the body forces, r the applied heat sources, p the pore pressure and $\mathbf{h}$ the heat flux vector. The above equations are formulated for an arbitrary material portion of continuum, occupying the volume Ω with the contour $\partial\Omega$ and the normal unitary vector $\mathbf{n}$. It is clearly evidenced in Eq.(4) the effect of the fluid mass through the pore pressure p and the fluid mass flux vector $\mathbf{w}$.

By introducing Eqs.(2)-(5) in Eq.(1), applying the Gauss's theorem to transform the surface integral of Eq.(4) into a volumetric one, taking into account infinitesimal strains and null body (and inertial) forces and assuming that Eq.(1) holds for any arbitrary part of Ω, the explicit form of the internal energy density for local dissipative porous material can be expressed as

$$\rho\dot{e} = \boldsymbol{\sigma} : \dot{\boldsymbol{\varepsilon}} - \nabla\cdot\left(h_f\mathbf{w}\right) + \rho r - \nabla\cdot\mathbf{h} \tag{6}$$

where $h_f = e_f^m + p/\rho_f$ is the fluid specific enthalpy, e_f^m the fluid internal energy per unit of mass and $\boldsymbol{\varepsilon}$ is the strain tensor.

3.2. Second Law of Thermodynamics

The Second Law of Thermodynamics, Eq.(7), states that the energy quality can only deteriorates, i.e. the amount of energy that can be efficiently converted into mechanical work irreversibly decreases, see Coussy (1995, 2004).

$$\dot{S} - Q_T \geq 0 \tag{7}$$

In this equation $\dot{S}$ represents the system entropy rate and Q_T the entropy flux. The terms in Eq.(7) are defined as

$$\dot{S} = \int_\Omega \left[\rho\dot{s} + \nabla\cdot\left(s_f^m\mathbf{w}\right)\right]\mathrm{d}\Omega \tag{8}$$

$$Q_T = -\int_{\partial\Omega}\frac{\mathbf{h}\cdot\mathbf{n}_s}{T}\mathrm{d}\partial\Omega + \int_\Omega\frac{\rho r}{T}\mathrm{d}\Omega \tag{9}$$

being s the internal entropy density, s_f^m the fluid internal entropy per unit of mass and T the absolute temperature. By replacing Eqs.(8)-(9) into Eq.(7) the weak form of the Second Law of Thermodynamic is obtained as

$$\int_\Omega\left[\rho\dot{s} + \nabla\cdot\left(s_f^m\mathbf{w}\right) + \nabla\cdot\left(\frac{\mathbf{h}}{T}\right) - \frac{\rho r}{T}\right]\mathrm{d}\Omega \geq 0 \tag{10}$$

Under consideration of the mass conservation principle,

$$\dot{m} = -\nabla\cdot\mathbf{w} \tag{11}$$

being $\dot{m}$ the total rate of the fluid mass content, the general form of the Clausius-Duhem inequality (CDI) for porous media may be obtained from Eqs. (6), (10) and (11) as

$$\int_\Omega\left[\boldsymbol{\sigma} : \dot{\boldsymbol{\varepsilon}} + g_f^m\dot{m} + \rho T\dot{s} - \rho\dot{e} + \mathbf{w}\cdot\left(\nabla s_f^m - \nabla h_f\right) - \frac{\mathbf{h}}{T}\cdot\nabla T\right]\mathrm{d}\Omega \geq 0 \tag{12}$$

Thereby, the enthalpy density per unit mass g_f^m of a fluid component filling the porous space is defined by Coussy (1995, 2004) as

$$g_f^m = e_f^m + \left(\frac{p}{\rho_f}\right) - T s_f^m = h_f - T s_f^m \tag{13}$$

4. Thermodynamics of gradient-based poroplastic materials

Based on the original proposal by Simo and Miehe (1992) for local inelastic media, its extension for gradient plasticity by Svedberg and Runesson (1997) and further by Mroginski et al. (2011) for isothermal gradient poroplasticity continua, arbitrary thermodynamic states of an open gradient poroplastic material under non-isothermal condition may be defined in terms of; the elastic strain tensor $\boldsymbol{\varepsilon}^e = \boldsymbol{\varepsilon} - \boldsymbol{\varepsilon}^p$, the elastic fluid mass content $m^e = m - m^p$, the elastic entropy $s^e = s - s^p$ and the internal variables q_α, with $\alpha = p, s$ corresponding to the solid or porous phase respectively. In these works, the internal variables are the only ones of non-local character.

Following the thermodynamically consistent gradient-regularized material theory for small strain kinematics by Svedberg and Runesson (1997); Vrech and Etse (2009) and Mroginski et al. (2011), a restricted form of non-local gradient theory is considered. Therefore, the internal energy density can be expressed as

$$e = e\left(\boldsymbol{\varepsilon}^e, m^e, s^e, q_\alpha, \nabla q_\alpha\right) \tag{14}$$

By replacing the time derivative of Eq.(14) in Eq.(12), and integrating the gradient term by parts, the weak form of the Clausius-Duhem inequality results

$$\int_\Omega \left[\left(\boldsymbol{\sigma} - \rho \frac{\partial e}{\partial \boldsymbol{\varepsilon}^e}\right) : \dot{\boldsymbol{\varepsilon}} + \left(g_f^m - \rho \frac{\partial e}{\partial m^e}\right) \dot{m} + \rho \left(T - \frac{\partial e}{\partial s^e}\right) \dot{s} + \rho \frac{\partial e}{\partial \boldsymbol{\varepsilon}^e} \dot{\boldsymbol{\varepsilon}}^p + \rho \frac{\partial e}{\partial m^e} \dot{m}^p + \rho \frac{\partial e}{\partial s^e} \dot{s}^p + \sum_\alpha Q_\alpha \dot{q}_\alpha + \mathbf{w} \cdot \left(\nabla s_f^m - \nabla h_f\right) - \frac{\mathbf{h} \cdot \nabla T}{T} \right] \mathrm{d}\Omega + \int_{\partial\Omega} Q_\alpha^{(b)} \dot{q}_\alpha \, \mathrm{d}\partial\Omega \geq 0 \tag{15}$$

being $Q_\alpha = Q_\alpha^l + Q_\alpha^{nl}$, with Q_α^l and Q_α^{nl} the local and non-local dissipative stresses in the domain Ω, respectively, and ${}^{(b)}Q_\alpha$ the dissipative stress on the boundary $\partial\Omega$.

$$Q_\alpha^l = -\rho \frac{\partial e}{\partial q_\alpha} \quad ; \quad Q_\alpha^{nl} = T \nabla \cdot \left(\frac{\rho}{T} \frac{\partial e}{\partial \nabla q_\alpha}\right) \quad ; \quad {}^{(b)}Q_\alpha = -\mathbf{n}_s \cdot \rho \frac{\partial e}{\partial \nabla q_\alpha} \tag{16}$$

As a result, Coleman's equations are formally obtained as in the case of the local continuum theory

$$\boldsymbol{\sigma} = \rho \frac{\partial e}{\partial \boldsymbol{\varepsilon}^e} \quad ; \quad T = \frac{\partial e}{\partial s^e} \quad ; \quad g_f^m = \rho \frac{\partial e}{\partial m^e} \tag{17}$$

Finally, from Eq.(15) the dissipations related to the plastic process, heat and fluid mass transports can be computed, respectively, as

$$\varphi^p = \boldsymbol{\sigma} : \dot{\boldsymbol{\varepsilon}}^p + g_f^m \dot{m}^p + \rho T \dot{s}^p + Q_\alpha \dot{q}_\alpha \quad ; \quad \varphi^{th} = -\frac{\mathbf{h} \cdot \nabla T}{T} \quad ; \quad \varphi^f = \mathbf{w} \cdot \left(\nabla s_f^m - \nabla h_f\right) \tag{18}$$

Due to the existence of gradient terms, a dissipative term on the boundary appears

$${}^{(b)}\varphi^{nl} = -\int_{\partial\Omega} \mathbf{n}_s \cdot \rho \frac{\partial e}{\partial \nabla q_\alpha} \dot{q}_\alpha \, \mathrm{d}\partial\Omega \tag{19}$$

Regarding gradient-based non-isothermal porous media, the following decomposition of the Helmholtz's free energy and the specific entropy may be assumed (Coussy, 1995)

$$\psi = e - T\, s = \psi_s + m\, \psi_f \quad ; \quad s = s_s + m\, s_f \tag{20}$$

where ψ_s is the total free energy related to the solid skeleton, ψ_f is the fluid-specific Helmholtz's free energy, s_s is the specific entropy related to the solid skeleton and s_f is the specific entropy related to the porous phase.

From the fluid state equations, the mathematical functions of the pore pressure p, s_f and $\dot{\psi}_f$ in terms of ψ_f can be obtained (Coussy, 2004) as

$$\frac{p}{\rho_f} = g_f^m - \rho\, \psi_f \quad ; \quad s_f = -\frac{\partial \psi_f}{\partial T} \quad ; \quad \dot{\psi}_f = \frac{\partial \psi_f}{\partial T} \dot{T} \tag{21}$$

Then, replacing Eqs.(20) and (21) in Eq.(12) the following expressions for the Coleman's relations are obtained

$$\boldsymbol{\sigma} = \rho \frac{\partial \psi_s}{\partial \boldsymbol{\varepsilon}^e} \quad ; \quad p = \rho \rho_f \frac{\partial \psi_s}{\partial m^e} \quad ; \quad s_s = -\frac{\partial \psi_s}{\partial T} \tag{22}$$

Dissipations related to the plastic process and to the heat and fluid mass transports can be computed as

$$\varphi^p = \boldsymbol{\sigma} : \dot{\boldsymbol{\varepsilon}}^p + \frac{p}{\rho_f} \dot{m}^p + Q_\alpha \dot{q}_\alpha \quad ; \quad \varphi^{th} = -\frac{\mathbf{h} \cdot \nabla T}{T} \quad ; \quad \varphi^f = \mathbf{w} \cdot \left(\nabla s_f^m - \nabla h_f \right) \tag{23}$$

where the corresponding dissipative stresses result

$$Q_\alpha^l = -\rho \frac{\partial \psi_s}{\partial q_\alpha} \quad ; \quad Q_\alpha^{nl} = T \nabla \cdot \left(\frac{\rho}{T} \frac{\partial \psi_s}{\partial \nabla q_\alpha} \right) \quad \text{in the domain } \Omega \tag{24}$$

The following additive expression of the Helmholtz's free energy corresponding to gradient poroplastic materials is adopted

$$\psi_s \left(\boldsymbol{\varepsilon}^e, m^e, \theta, q_\alpha, \nabla q_\alpha \right) = \psi^e \left(\boldsymbol{\varepsilon}^e, m^e, \theta \right) + \psi^l \left(q_\alpha, \theta \right) + \psi^{nl} (\nabla q_\alpha) \tag{25}$$

whereby ψ^e represents the elastic free energy, ψ^l is the local plastic energy and ψ^{nl} is the non-local plastic one. Also $\theta = T - T_0$ is the relative temperature. Neglecting the initial and inertial forces, the elastic term is defined as follows

$$\rho \psi^e = \frac{1}{2} \boldsymbol{\varepsilon}^e : \mathbf{C} : \boldsymbol{\varepsilon}^e + \frac{1}{2} M \left(\frac{m^e}{\rho_f} \right)^2 - \frac{1}{2} \chi \theta^2 + \aleph m^e \theta - \frac{m^e}{\rho_f} M \mathbf{B} : \boldsymbol{\varepsilon}^e - \theta \mathbf{A} : \boldsymbol{\varepsilon}^e \tag{26}$$

being $\mathbf{C}$ the fourth order elastic tensor, M the Biot's modulus, χ the concrete heat capacity, $\aleph$ the latent heat of variation in fluid mass content, $\mathbf{B} = b\mathbf{I}$ the Biot's tensor with b the Biot's coefficient and $\mathbf{I}$ the second order identity tensor, and $\mathbf{A} = \alpha_\theta \mathbf{I}$ the thermal expansion tensor, with α_θ the thermal expansion coefficient.

The Helmholtz's free energy component corresponding to the local portion of the poroplastic behavior turns

$$\rho \psi^l = \frac{H_\alpha^l}{2} q_\alpha^2 - \theta s_{fr}^{(q_\alpha)} \tag{27}$$

thereby the first term represents the frozen free energy, since it is the free energy recovered after restoring the initial temperature, stress and fluid enthalpy, meanwhile $s_{fr}^{(q_\alpha)}$ represents the unrecovered entropy, called the frozen entropy (Coussy, 1995).

Regarding gradient-based non-isothermal poroplastic materials, the non local free energy may be assumed as

$$\rho \psi^{nl} = \frac{1}{2} l_c^2 \, \nabla q_\alpha \cdot \mathbf{H}_\alpha^{nl} \cdot \nabla q_\alpha \tag{28}$$

In the above equations, H_α^l is the local-plastic hardening/softening modulus, $\mathbf{H}_\alpha^{nl}$ the gradient softening second-order tensor and l_c the gradient characteristic length.

In the particular case of gradient isotropy, the gradient softening second-order tensor can be expressed as

$$\mathbf{H}_\alpha^{nl} = H_\alpha^{nl} \mathbf{I} \tag{29}$$

being H_α^{nl} a positive non-zero scalar.

For l_c three alternative definitions can be given, see Svedberg (1999). On the one hand, it can be defined as a convenient dimensional parameter. On the other hand, as a physical entity that characterizes the material microstructure. Alternatively, l_c can be interpreted as an artificial numerical stabilization mechanism for the non-local theory.

5. Constitutive equations of thermodynamically consistent gradient poroplastic materials under non-isothermal conditions

In this section the constitutive equations are developed for thermodynamically consistent gradient poroplastic materials subjected to non-isothermal conditions. Furthermore, expressions for the heat conductivity, the fluid flux and the non-local poroplastic flow rule are formulated.

5.1. Constitutive equations

From Eqs.(22), (26) and (27), the constitutive equations in terms of the total stresses, the pore pressure and the fluid-specific internal entropy may be derived as

$$\boldsymbol{\sigma} = \mathbf{C} : \boldsymbol{\varepsilon}^e - M\frac{m^e}{\rho_f}\mathbf{B} - \theta\mathbf{A} \tag{30}$$

$$p = \frac{M}{\rho_f}m^e - M\mathbf{B} : \boldsymbol{\varepsilon}^e + \rho_f\aleph\theta \tag{31}$$

$$s_s = \mathbf{A} : \boldsymbol{\varepsilon}^e - \aleph m^e + \chi\theta + s_{fr}^{(q_\alpha)} \tag{32}$$

From Eq.(24), and after some algebra, the thermodynamically consistent dissipative stresses for local and non-local porous media result

$$Q_\alpha^l = -H_\alpha^l q_\alpha + \theta\frac{\partial s_{fr}^{(q_\alpha)}}{\partial q_\alpha} \quad ; \quad Q_\alpha^{nl} = l_c^2\left(-\frac{\nabla T}{2T}\cdot\mathbf{H}_\alpha^{nl}\cdot\nabla q_\alpha + \mathbf{H}_\alpha^{nl} : \nabla^2 q_\alpha\right) \tag{33}$$

Note in Eq.(33-a) that under a temperature variation, the local plastic dissipative stresses and consequently the yield surface may vary, even if no plastic loading occurs.

5.2. Heat conduction and fluid transport

Based on the weak form of the Second law of Thermodynamics, Eq.(10), the heat equation for an open porous medium results

$$T\dot{s} = -\nabla\cdot\mathbf{h} + r + \varphi_M \tag{34}$$

where the mechanical dissipation $\varphi_M = \varphi^p + \varphi^f$, with φ^p and φ^f the plastic and fluid dissipations, respectively. For heat conduction description, the Fourier law is considered, i.e. $\mathbf{h} = -k_d\nabla\theta$, being k_d the concrete conductivity. In case of cementitious materials, the internal heat production due to mechanical dissipations r, is quite small and can be neglected (Ulm and Coussy, 1999). Also, the heat convectively transported by fluid and the heat source due to the viscous dissipation are neglected. The reason for this is that their orders of magnitude are very small in comparison with the heat supplied by diffusion through the porous medium (Obeid et al., 2001). Consequently, Eq.(34) becomes

$$T\dot{s} = k_d\nabla\cdot\nabla T \tag{35}$$

From the fluid dissipation in Eq.(23-c) it is possible to obtain a suitable expression for the conduction law of fluid masses, leading to the Darcy law

$$\frac{\mathbf{w}}{\rho_f} = -k_w\nabla p \tag{36}$$

being k_w the permeability coefficient.

5.3. Non-local poroplastic flow rule

Rate equations for the internal variables are defined in the same way as for local plasticity. Therefore, for the general non-associated flow rule and hardening/softening laws, the dissipative potential Φ^* is introduced and the rates of the plastic strains tensor, the plastic mass and the internal variables are defined as

$$\dot{\boldsymbol{\varepsilon}}^p = \dot{\lambda}\frac{\partial\Phi^*}{\partial\boldsymbol{\sigma}}; \qquad \dot{m}^p = \dot{\lambda}\frac{\partial\Phi^*}{\partial p}; \qquad \dot{q}_\alpha = \dot{\lambda}\frac{\partial\Phi^*}{\partial Q_\alpha} \tag{37}$$

where $\dot{\lambda}$ is the rate of the plastic multiplier. To complete the constitutive formulation, the Kuhn-Tucker conditions are introduced

$$\dot{\lambda} \geq 0, \quad \Phi(\boldsymbol{\sigma}, p, \theta, Q_\alpha) \leq 0, \quad \dot{\lambda}\Phi(\boldsymbol{\sigma}, p, \theta, Q_\alpha) = 0 \tag{38}$$

being Φ the yield function.

5.4. Non-local poroplastic consistency

Given the consistency condition

$$\dot{\Phi} = \frac{\partial \Phi}{\partial \boldsymbol{\sigma}} : \dot{\boldsymbol{\sigma}} + \frac{\partial \Phi}{\partial p}\dot{p} + \frac{\partial \Phi}{\partial Q_\alpha}\dot{Q}_\alpha + \frac{\partial \Phi}{\partial \theta}\dot{\theta} = 0 \tag{39}$$

from Eqs.(30),(32), (37) and (39), the following differential equation for the plastic multiplier is obtained

$$\dot{\lambda}\left(h + h^{nl}\right) + \dot{\Phi}^{nl} + \dot{\Phi}^{trial} = 0 \tag{40}$$

where h and h^{nl} are the generalized local and gradient plastic modulus, respectively. Also, $\dot{\Phi}^{trial}$ and $\dot{\Phi}^{nl}$ the rates of the local and gradient loading functions, respectively. These values are defined as

$$h = -\frac{\partial \Phi}{\partial \boldsymbol{\sigma}} : \boldsymbol{C} : \frac{\partial \Phi^*}{\partial \boldsymbol{\sigma}} + \frac{M}{\rho_f}\frac{\partial \Phi}{\partial \boldsymbol{\sigma}} : \boldsymbol{B}\frac{\partial \Phi^*}{\partial p} - \frac{M}{\rho_f}\frac{\partial \Phi}{\partial p}\frac{\partial \Phi^*}{\partial p} + M\frac{\partial \Phi}{\partial p}\boldsymbol{B} : \frac{\partial \Phi^*}{\partial \boldsymbol{\sigma}} + \theta\frac{\partial^2 S^f}{\partial^2 q_\alpha}\frac{\partial \Phi}{\partial Q_\alpha}\frac{\partial \Phi^*}{\partial Q_\alpha} - H^l\frac{\partial \Phi}{\partial Q_\alpha}\frac{\partial \Phi^*}{\partial Q_\alpha} \tag{41}$$

$$h^{nl} = 2l_c^2\frac{\partial \Phi}{\partial Q_\alpha}\frac{\partial^2 \Phi^*}{\partial^2 Q_\alpha}\mathbf{H}^{nl}\cdot\nabla q_\alpha\cdot\nabla Q_\alpha - \frac{l_c^2}{2\theta}\frac{\partial \Phi}{\partial Q_\alpha}\frac{\partial^2 \Phi^*}{\partial^2 Q_\alpha}\nabla\theta\cdot\mathbf{H}^{nl}\cdot\nabla Q_\alpha \tag{42}$$

$$\dot{\Phi}^{nl} = -\frac{l_c^2}{2\theta}\frac{\partial \Phi}{\partial Q_\alpha}\mathbf{H}^{nl}\cdot\nabla q_\alpha\cdot\nabla\dot{\theta} + \frac{l_c^2}{2\theta}\frac{\partial \Phi}{\partial Q_\alpha}\nabla\theta\cdot\mathbf{H}^{nl}\cdot\nabla q_\alpha\cdot\dot{\theta} + 2l_c^2\frac{\partial \Phi}{\partial Q_\alpha}\frac{\partial \Phi^*}{\partial Q_\alpha}\mathbf{H}^{nl}\cdot\nabla q_\alpha\cdot\nabla\dot{\lambda} + \\ - \frac{l_c^2}{2\theta}\frac{\partial \Phi}{\partial Q_\alpha}\frac{\partial \Phi^*}{\partial Q_\alpha}\nabla\theta\cdot\mathbf{H}^{nl}\cdot\nabla\dot{\lambda} \tag{43}$$

$$\dot{\Phi}^{trial} = -\frac{\partial \Phi}{\partial \boldsymbol{\sigma}}\mathbf{C} : \dot{\boldsymbol{\varepsilon}} - \frac{M}{\rho_f}\frac{\partial \Phi}{\partial \boldsymbol{\sigma}} : \mathbf{B}\dot{m} + \frac{\partial \Phi}{\partial \boldsymbol{\sigma}} : \mathbf{A}\dot{\theta} + \frac{M}{\rho_f}\frac{\partial \Phi}{\partial p}\dot{m} - \frac{\partial \Phi}{\partial p}M\mathbf{B} : \dot{\boldsymbol{\varepsilon}} + \frac{\partial \Phi}{\partial p}\rho_f\chi\dot{\theta} + \left(\frac{\partial s_{fr}^{(q_\alpha)}}{\partial q_\alpha}\frac{\partial \Phi}{\partial \theta}\right)\dot{\theta} \tag{44}$$

6. Thermodynamic constitutive model for non-local poroplastic materials like concrete

In this section, the gradient-based model for concrete proposed by Vrech and Etse (2009) is extended to account for the temperature effects in the framework of the previously discussed thermodynamically consistent gradient-based theory for poroplastic materials.

6.1. Maximum Strength Criterion

The maximum strength criterion of the proposed temperature-dependent Leon-Drucker-Prager criterion (TD-LDP) arises from the combination between the compressive meridian of the Leon criterion, see Leon (1935), and the deviatoric description of the Drucker-Prager criterion. The TD-LDP criterion is defined in the space of effective stresses to account for the poromechanical material description of the proposed model. The TD-LDP failure surface is defined as

$$\Phi({}^*\sigma', {}^*\tau, \theta) = \alpha(\theta)\,\frac{3}{2}\,{}^*\tau^2 + \beta(\theta)\,m_0\left(\frac{{}^*\tau}{\sqrt{6}} + {}^*\sigma'\right) - c_0 = 0 \tag{45}$$

where

$$\sigma' = \frac{I_1}{3} - p \quad ; \quad \tau = \sqrt{2J_2} \quad \rightarrow \quad {}^*\sigma' = \frac{\sigma'}{f_c'} \quad ; \quad {}^*\tau = \frac{\tau}{f_c'} \tag{46}$$

being σ' and τ the Haigh Westergaard effective volumetric and deviatoric stress coordinates, respectively. I_1 is the first invariant of total stress tensor, J_2 is the second invariant of deviatoric stress tensor, and f_c' and f_t' are the uniaxial

compressive and tensile strengths, respectively. The friction and cohesion of the virgin material, m_0 and c_0, are calibrated at room temperature as

$$m_0 = \frac{3}{2}\frac{\left(f_c'^2 - f_t'^2\right)}{f_c' f_t'} \quad ; \quad c_0 = 1 \tag{47}$$

The temperature-dependent functions $\alpha(\theta)$ and $\beta(\theta)$ vary according to

$$\alpha(\theta) = (1 - \gamma_1\theta)^{(-1)} \quad ; \quad \beta(\theta) = (1 - \gamma_2\theta)\,(1 - \gamma_1\theta)^{(-1)} \tag{48}$$

where γ_1 and γ_2 are coefficients to be calibrated depending on the particular concrete quality. Moreover, γ_1 is always positive, and $\gamma_1\theta < 1$, so $\alpha > 1$ and it increases with the temperature.

To have a more clear understanding of the physical meaning of the temperature depending functions, Eq.(45) is rewritten in the form

$$\Phi({}^*\sigma', {}^*\tau, \theta) = \frac{3}{2}\,{}^*\tau^2 + \frac{\beta(\theta)}{\alpha(\theta)}\, m_0 \left(\frac{{}^*\tau}{\sqrt{6}} + {}^*\sigma'\right) - \frac{c_0}{\alpha(\theta)} = 0 \tag{49}$$

so, $c = c_0/\alpha$ may be considered as the degradated cohesion due to temperature, with α representing the cohesion degradation parameter caused by temperature.

On the other hand, as $\beta/\alpha = (1 - \gamma_2\theta) < 1$, then $m = (\beta/\alpha)m_0$ may be considered as the degraded friction due to temperature, which decreases with increasing temperature. So, from the physical stand point, both temperature dependent coefficients α and β in Eq.(45) represent the degradation of the fundamental concrete mechanical properties, i.e., the cohesion and friction under increasing temperature. These functions, and particularly the coefficients γ_1 and γ_2, can be easily calibrated from experimental results on concrete probes under different temperatures and considering different concrete qualities.

The evolution of the failure surface in the compressive meridian with variable temperature levels is shown in Fig.(2). With increasing temperatures, the failure surface decreases non isotropically, signalizing both cohesion and friction degradations.

6.2. Yield condition and plastic potential

Beyond the elastic regime, plastic strains take place and the material exhibit hardening or softening. To capture the diverse inelastic behaviors, one single equation-based yield surface is proposed.

$$\Phi({}^*\sigma', {}^*\tau, \theta, {}^h Q, {}^s Q) = \alpha(\theta)\,\frac{3}{2}{}^*\tau^2 + {}^h Q\,\beta(\theta)\, m_0 \left(\frac{{}^*\tau}{\sqrt{6}} + {}^*\sigma'\right) - {}^h Q\,{}^s Q = 0 \tag{50}$$

Furthermore, the following plastic potential surface is adopted to reduce the excessive volumetric dilatation of concrete in the low confinement regime

$$\Phi^*({}^*\sigma', {}^*\tau, \theta, {}^h Q, {}^s Q) = \alpha(\theta)\,\frac{3}{2}{}^*\tau^2 + \beta(\theta)\, m_0 \left(\frac{{}^*\tau}{\sqrt{6}} + \eta\,{}^*\sigma'\right) - {}^h Q\,{}^s Q = 0 \tag{51}$$

being η the volumetric non-associativity degree which varies between $0 \le \eta \le 1$. The extreme case when $\eta = 0$ corresponds to the isochoric plastic flow, while $\eta = 1$ results in associated plasticity.

The evolution of the yield and plastic potential surfaces in pre-peak regime is controlled by the hardening dissipative stress ${}^h Q_0 \le {}^h Q \le 1$, while the softening dissipative stress remains constant ${}^s Q = 1$. When ${}^h Q = 1$ the TD-LDP criterion is reached. The strength degradation during softening regime, when ${}^h Q = 1$, is defined by the evolution of ${}^s Q$ which continuously reduces as the local and non-local decohesion process develops from its maximum value down to ${}^s Q = 0$.

6.3. Thermodynamic consistency in pre-peak regime

Independently of the acting temperature, concrete exhibits hardening in pre-peak regimen. This continuous stiffness degradation is related to homogeneously distributed processes of inelastic deformation which can be realistically modeled by means of local hardening rules.

The inelastic local free energy density controling the hardening response of concrete during coupled thermo-mechanical processes is defined as

$$\rho\, {}^{h}\psi = -{}^{h}Q_0\, {}^{h}q + \frac{0.9}{\chi_h} cos\left(\chi_h\, {}^{h}q\right) \tag{52}$$

where ${}^{h}q$ represents the scalar hardening variable. As it is shown in Eq.(53), χ_h can be interpreted as a hardening ductility measure depending on both, the normalized confining pressure and the temperature.

$$\chi_h = -\frac{\pi}{2}\frac{\|\mathbf{m}\|}{x_p} \quad \text{with} \quad x_p({}^{*}\sigma', \theta) = A_h\, exp\left(B_h\, {}^{*}\sigma' + C_h\, \theta\right) \tag{53}$$

being A_h, B_h and C_h internal parameters to be calibrated by experimental tests under low, medium and high confinements at normal and high temperatures, and $\mathbf{m}$ the gradient tensor perpendicular to the plastic potential.

The expression of the dissipative stress ${}^{h}Q$ is obtained from Eq.(52) as

$${}^{h}Q = -\rho\frac{\partial\, {}^{h}\psi}{\partial\, {}^{h}q} = {}^{h}Q_0 + 0.9 sin\left(\chi_h\, {}^{h}q\right) \tag{54}$$

The variation of ${}^{h}Q$ in terms of T is shown in Fig.(3).

$${}^{h}\dot{q} = \dot{\lambda}\frac{\partial\Phi^{*}}{\partial\, {}^{h}Q} = -\dot{\lambda} \tag{55}$$

From Eqs. (54) and (55) the hardening evolution law is obtained as

$${}^{h}\dot{Q} = -\rho\frac{\partial^2\, {}^{h}\psi}{\left(\partial\, {}^{h}q\right)^2}\, {}^{h}\dot{q} - \rho\frac{\partial^2\, {}^{h}\psi}{\partial\, {}^{h}q\, \partial\theta}\, \dot{\theta} \quad \rightarrow \quad {}^{h}\dot{Q} = {}^{h}H^{l}\, \dot{\lambda} + {}^{h}H^{\theta}\dot{\theta} \tag{56}$$

with the hardening plastic modulus computed as

$${}^{h}H^{l} = \rho\frac{\partial^2\, {}^{h}\psi^{l}}{\left(\partial\, {}^{h}q\right)^2} = -0.9\chi_h\, cos\left(\chi_h\, {}^{h}q\right) \tag{57}$$

and the hardening thermal modulus computed as

$${}^{h}H^{\theta} = \rho\frac{\partial^2\, {}^{h}\psi^{l}}{\partial\, {}^{h}q\ \partial\,\theta} = 0.9\, {}^{h}q\ cos\left(\chi_h\, {}^{h}q\right)\frac{\partial\chi_h}{\partial\theta} \quad \text{being} \quad \frac{\partial\chi_h}{\partial\theta} = -\frac{\pi}{2}\frac{\|\mathbf{m}\|}{{x_p}^2}\frac{\partial x_p}{\partial\theta} \tag{58}$$

6.4. Thermodynamic formulation of softening rule

Softening behavior of concretes under high temperatures is related to deformation processes under increasing inhomogeneities. The instantaneous concrete strength in softening regime is obtained by means of two parallel mechanisms: the remaining strength for further fracture development in the active cracks, which is defined by a temperature dependent fracture energy-based mechanism, and the remaining strength for further mechanical/thermal degradations in the material located in between cracks. The last one is defined by a gradient-based mechanism. Thus, the total inelastic free energy density controling the softening behavior of concrete under coupled thermo-mechanical process beyond the peak strength can be mathematically expressed as

$${}^{s}\psi = {}^{s}\psi^{l} + {}^{s}\psi^{nl} \tag{59}$$

being ${}^{s}\psi^{l}$ the local or fracture-based free energy density component and ${}^{s}\psi^{nl}$ the non-local or gradient-based one. Both are temperature dependent. The first one represents the energy released in an elastoplastic continuum, equivalent to

the discontinuous with the same fractured height, which is obtained through an homogenization process according to the fracture energy-based plasticity model by Willam et al. (1985) and Willam and Etse (1990)

$$ {}^{s}\psi^{l} = -\frac{1}{\rho\,\alpha_f}\exp\left(\alpha_f\,{}^{s}q\right) \quad , \quad \alpha_f = 5\frac{h_f^{\theta}}{u_r}\,\|\langle\mathbf{m}\rangle\| \tag{60} $$

being ${}^{s}q$ the scalar softening variable. The gradient tensor to the plastic potential is computed as

$$ \mathbf{m} = \frac{\partial\Phi^{*}}{\partial\boldsymbol{\sigma}'_{\boldsymbol{I}}} \tag{61} $$

while u_r represents the maximum crack opening displacement in mode I type of failure and $\boldsymbol{\sigma}'_I$ the tensor of principal effective stresses. The Mc Auley brackets in Eq.(60-b) indicate that only tensile principal plastic strains contribute to the energy density during the fracture evolution process.

The fracture energy-based characteristic length h_f^{θ} defines the distance between macrocracks. In this model formulation, h_f^{θ} is controlled by both the temperature dependent characteristic fracture length h_t^{θ} (in mode I type of fracture), and the normalized pressure-dependent function $R_G({}^{*}\sigma')$.

$$ h_f^{\theta}\,({}^{*}\sigma',\theta) = \frac{h_t^{\theta}}{R_G({}^{*}\sigma')} \quad \text{with} \quad h_t^{\theta} = h_t\,exp\,(A_t\theta) \tag{62} $$

and

$$ R_G\,({}^{*}\sigma') = \begin{cases} 1 & {}^{*}\sigma' \geq 0, \\ C_u + D_u\,sin\left(2\,{}^{*}\sigma' - \frac{\pi}{2}\right), & 0 \geq {}^{*}\sigma' \geq -1.5, \\ 100, & {}^{*}\sigma' \leq -1.5. \end{cases} \tag{63} $$

where A_t, C_u and D_u are constants to be calibrated from experimental results and h_t is the characteristic length in mode I type of fracture at room temperature. As can be observed in Eq.(63), R_G continuously increases under increasing confinement pressure ${}^{*}\sigma'$, see Fig.(4). The increase of R_G leads to the reduction of the distance between microcracks as represented by h_f^{θ} in Eq.(62) and, consequently to a more diffused type of failure.

The local or fracture energy-based dissipative stress ${}^{s}Q^{l}$ takes the form

$$ {}^{s}Q^{l} = -\rho\frac{\partial\,{}^{s}\psi^{l}}{\partial\,{}^{s}q} = \exp\,(\alpha_f\,{}^{s}q) \tag{64} $$

and its evolution law can be obtained as

$$ {}^{s}\dot{Q}^{l} = {}^{s}H^{l}\dot{\lambda} + {}^{s}H^{\theta}\,\dot{\theta} \tag{65} $$

with the local softening thermo-plastic modulus

$$ {}^{s}H^{l} = \rho\frac{\partial^2\,\psi^{l}}{(\partial\,{}^{s}q)^2} = -\alpha_f\exp\left(\alpha_f\,{}^{s}q\right) \tag{66} $$

and the local softening thermal modulus

$$ {}^{s}H^{\theta} = \rho\frac{\partial^2\,\psi^{l}}{\partial^{s}q\,\partial\theta} = {}^{s}q\exp\left(\alpha_f\,\|\langle\mathbf{m}\rangle\|\right)\frac{\partial\alpha}{\partial\theta}\dot{\theta} \tag{67} $$

with

$$ \frac{\partial\alpha}{\partial\theta} = \frac{5}{u_r}\,\|\langle\mathbf{m}\rangle\|\,\frac{\partial h_f^{\theta}}{\partial\theta} \tag{68} $$

The non-local component of the inelastic free energy density

$$ {}^{s}\psi^{nl}\left(\nabla {}^{s}q\right) = \frac{1}{2\rho} l_c^2 \, {}^{s}H^{nl} \, \nabla^2 \left({}^{s}q\right) \tag{69} $$

is expressed in terms of the gradient perpendicular to the scalar softening state variable $\nabla {}^{s}q$, the gradient modulus ${}^{s}H^{nl}$ and the thermo-plastic gradient characteristic length l_c, which defines the width of the inelastic process in the material located between cracks in terms of the temperature and the acting confining pressure. Summarizing, l_c considers the influence of the pore pressure as defined by Mroginski and Etse (2013) but extended to take into account temperature effects according to

$$ l_c({}^{*}\sigma', \theta) = \begin{cases} 0 & {}^{*}\sigma' \geq 0, \\ E_l l_{c,m} \left(1 + D_l\right) \left[1 + sin\left(F_l \left(1 + C_l \theta\right) - \frac{\pi}{2}\right)\right], & 0 \leq {}^{*}\sigma' \leq -1.5, \\ l_{c,m} \left(1 + D_l \theta\right), & -1.5 \geq {}^{*}\sigma' \end{cases} \tag{70} $$

being l_{cm} the maximum possible internal length and C_l, E_l, D_l and F_l the internal parameters that appropriately define the variation of l_c with the temperature and effective confinement. Its variation can be seen in Fig.(5).

From Eq. (24-b), the non-local dissipative stress in softening results

$$ {}^{s}Q^{nl}(\nabla \, {}^{s}q) = \nabla \cdot \rho \frac{\partial \, \psi^{nl}}{\partial \left(\nabla \, {}^{s}q\right)} = l_c^2 \, {}^{s}H^{nl} \, \nabla^2 \, {}^{s}q = -l_c^2 \, {}^{s}H^{nl} \, \nabla^2 \lambda \tag{71} $$

and its evolution law yields

$$ {}^{s}\dot{Q}^{nl} = -l_c^2 \, {}^{s}H^{nl} \, \nabla^2 \dot{\lambda} \tag{72} $$

The total dissipative stress in softening regime is obtained from the addition of Eq.(64) and (71).

6.5. Summary of material parameters

In summary, ten parameters are required to define initial stiffness, strength criterion, initial yield as well as the fracture energy and the gradient-based softening formulation of the proposed model. The initial young modulus E_0 and the Poisson's ratio ν define the elastic material features. The elastic limit coincident with the initial yield surface is characterized by the initial hardening parameter ${}^{h}Q_0$. Maximum strength criterion is described by the uniaxial compressive and tensile strengths f_c' and f_t' respectively, and the temperature level θ.

The maximum crack opening displacement u_r can be experimentally obtained from the fracture energy released in mode I type of failure G_f', while h_t represents the specimen height in the uniaxial tensile test. The parameters related to the gradient-based softening formulation are the gradient modulus ${}^{s}H^{nl}$ and the amplitude of the gradient characteristic length l_{cm}.

In addition, the material model includes three internal functions corresponding to hardening ductility and softening internal lengths, see Eqs.(53), (63) and (70). The experimental results by Hurlbut (1985) were used to calibrate the temperature independent parameters of the proposed constitutive model. These experiments were performed on concrete specimens at normal temperatures subjected to uniaxial tensile and compression tests as well as to triaxial compressive tests. Basic material properties of concrete used by Hurlbut (1985) are given in Table (1).

Table 1: Concrete Properties

Elasticity Modulus - E_0	19300 MPa
Poisson Modulus - υ	0.20
Compressive Strength - f_c'	22.00 MPa
Tensile Strength - f_t'	2.20 MPa
Tensile rupture displacement - u_r	0.127 mm

The experimental results of uniaxial compressive tests on concrete specimens at different temperatures by Lee et al. (2008) were considered to calibrate the temperature dependent parameters of the model, particularly γ_1 and γ_2. Table (2) summarizes the resulting material parameters of the model.

Table 2: Model Parameters

Initial hardening parameter - ${}^{h}Q_0$	0.10
Maximum gradient characteristic length - l_{cm}	110 mm
Gradient Modulus - ${}^{s}H^{nl}$	1.00 MPa
Temperature independent fracture energy-based characteristic length - h_t	108.00 mm
Maximum strength coefficients - γ_1; γ_2	0.00126; 0.00056
Hardening ductility coefficients - A_h; B_h; C_h	0.0007; -0.0089; 0.0063
Coefficients for temp. dependency of fracture energy-based charact. length - A_t; C_u; D_u	-2.20; 51; 50
Gradient characteristic length coefficients - D_l; E_l; F_l	0.20; 0.50; 2.00

6.6. Temperature-dependent Concrete Elasticity Modulus

The concrete elasticity modulus plays a very important role in the overall temperature dependent response behavior of concrete predicted by the proposed model. With the aim to define an accurate dependence function of this modulus on the acting temperature, several experimental results were evaluated in this research. As a consequence, the dependency of the concrete elasticity modulus E on the temperature level θ is approximated with the lineal function

$$E = E_0 (1 - \alpha_E \theta) \tag{73}$$

being E_0 the elasticity modulus at 20°C and $\alpha_E = 0.0014$, a degradation parameter. Experimental data obtained from Anderberg and Thelandersson (1976); Diederichs et al. (1988); Castillo and Durrani (1990); Baker (1996); Della Croce et al. (2000); Janotka and Bagel (2002); Zhang and Bicanic (2002); Chang et al. (2006); Lee et al. (2008); Zhang (2011) of the ratio E/E_0 corresponding to the temperature range between 20°C and 800°C are summarized in Fig.(6). As can be observed, the numerical approximation of the E/E_o ratio agrees very well with the experimental data.

7. Numerical Analyses

In this section, numerical predictions of concrete failure processes obtained with the proposed constitutive theory are evaluated when the specimen is subjected to combined thermo-mechanical actions. Firstly, the attention focuses on numerical simulations of experimental tests performed on hardened concrete specimens subjected to uniaxial compression under different and homogeneous temperature profiles. Then, numerical analyses of concrete failure behaviors are performed when the specimen is subjected to uniaxial tensile and triaxial compression tests under different temperature conditions.

In the computational analyses performed in this work, the dual mixed FE formulation for thermodynamically consistent gradient plasticity proposed by Vrech and Etse (2007, 2009) is considered, which is based on the original formulation by Svedberg and Runesson (1997) for gradient-regularized plasticity coupled with damage. It should be noted that the CST FE formulation for gradient plasticity used in this work leaded to very stable numerical performance even in case of localized failure modes. Although the consistent material tensor was not developed, the rate of convergence was higher than linear (tolerance of 1.00xE-4 was always achieved within a limited number of iterations). The considered material properties are those indicated in Tables (1) and (2). In Fig.(7) the overall geometry and boundary conditions of the cylindrical concrete specimen considered in the current numerical analyses are depicted. Due to the double symmetry of the problem, only one quarter of the concrete specimens is discretized. Inhomogeneous boundary conditions are introduced by imposing zero horizontal displacements to the nodes located on top of the specimen. Fig.(7) also illustrates the different finite element meshes considered in the numerical analyses.

Firstly, Firstly, model predictions are compared with experimental results of uniaxial compression tests obtained by Lee et al. (2008) on cylindrical concrete specimens of 101.6mm x 203.2mm. The material properties summarized in Table (1) were considered. In order to obtain comparable results, the finest regular discretization of Fig.(7) is used with the dimensions of specimens by Lee et al. (2008).

In Fig.(8) the numerical predictions in terms of axial stresses vs. axial strains are compared with the experimental results by Lee et al. (2008). The numerical predictions agree very well with the experimental data for all different temperature levels (from 20°C to 600°C), regarding the loss of both, stiffness in pre-peak regime and peak strength with increasing temperature. Another effect that can be clearly recognized from the experimental and numerical results in Fig.(8) is the relevant increment of the ductility (with respect to the reduced peak strength) in both the pre- and post-peak regimes as the temperature increases. In Fig.(9) model predictions can be observed for uniaxial compression tests on concrete probes under many different temperatures from 20 to 700°C, in terms of both axial and lateral strains. Actually, the experimental and numerical post peak branches of the uniaxial compression tests by Lee et al. (2008) in Fig. (8) suggest a very interesting effect of the temperature on concrete mechanical behavior. At low and medium temperature levels (up to approximately 400°C) the area below the stress-strain curve, representing the energy released (under mode II type of fracture) seems to be larger than that corresponding to 20°C (room temperature). However, and due to the relevant strength degradation, the energy released is smaller than the one at room temperature when concrete is subjected to high temperature levels.

In this work a more detailed analyses was performed for the variation of G_f^I (energy released in mode I or tensile mode) with respect to the acting temperature. In the proposed model formulation, the energy released in mode II type of failure is controlled by the energy released in mode I, see Eq.(62). Normalized values of G_f^I were evaluated at different temperatures with respect to the same energy of the uniaxial tensile test performed at room temperature ${}^oG_f^I$. The results are compared with the set of experimental data obtained from the literature, (Baker, 1996; Zhang and Bicanic, 2002; Nielsen and Bicanic, 2003; Menou et al., 2006; Zhang, 2011), and they are depicted in Fig.(10). In the same figure, the variation of the ratio $G_f^I/{}^oG_f^I$ as predicted by the proposed model is illustrated for the entire temperature range from 20 to 700°C. It can be observed that the experimental trend is very well reproduced by the proposed model. In other words, the normalized fracture energy released in mode I, increases up to a temperature level of about 400°C, and then it strongly and continuously decreases with increasing temperature.

Next the predictions of the proposed model of uniaxial tensile tests under different temperature conditions are shown in Fig.(11). The case of room temperature is compared with the uniaxial tensile test by Hurlbut (1985). By comparing the results in Figs.(9) and (11) it can be concluded that the tensile strength of concrete is more sensitive to temperature than the compressive one.

It is very interesting to evaluate the effect of the lateral confinement in triaxial compression tests performed on concretes damaged by temperature. In Fig.(12) the results obtained by Hurlbut (1985) for the traixial compression tests under room temperature at different confinements are compared with the results obtained with the model at 20 °C. Later, in Fig.(13), the model predictions for the triaxial compression tests design by hurbult, are re-evaluated for concrete with temperature damage of 500°C. When comparing these results with the ones in Fig.(9) it can be concluded that the confinement pressure contributes to reduces not only the lateral dilatancy of concrete, but mainly the strength degradation caused by temperature.

Next, the temperature effect on the failure pattern predicted by the proposed constitutive model is evaluated. Fig. (14) compares the equivalent plastic strain distributions at final stage of uniaxial compression tests performed at 20 °C and 500°C. The temperature dependent non-local degradation mechanisms included in the model through the gradient characteristic length is activated when the temperature increases. This leads to a strong stress redistribution of the critical stresses and, consequently, to an enlargement of the width of the strain localization band. This can be concluded from the comparison between the plastic strain distribution at residual stress of the 20°C and 500°C uniaxial compression tests in Fig.(14). In the load-displacement diagram, this effect corresponds to a more ductile failure behavior in the post peak regime of the 500°C test as compared to that of the 20°C, see Fig.(9). Following, the combined effect of the confinement pressure and temperature on the failure pattern of concrete cylinders under triaxial compression tests is evaluated. In Fig.(15) it can be observed the plastic strain distributions of the triaxial compression tests (under medium confinement) when subjected to 20°C and 500°C. Comparing the results of Fig.(15) and Fig.(14) it can be concluded that the damage due to thermal effects reduces the sensitivity of the concrete failure behavior respect to the confinement pressure. At residual strain stage under 500°C, the difference in the shear band width (represented by the equivalent plastic strain distribution) between the uniaxial compression test and the triaxial

compression test under medium confinement is much smaller than that corresponding to the same tests under 20°C.

Finally, the post-peak regularization capabilities of the proposed model for concrete failure behavior under temperature effect are evaluated. Fig. (16) shows the plastic strain distributions at residual stress of the uniaxial compression tests under 500°C corresponding to four different discretizations. The considered FE-meshes do not only vary in the finite element density (size) but also in their orientations. The equivalent plastic strain distributions of all four FE-meshes agree very well, demonstrating the regularization capabilities of the model. As can be noticed in Fig.(17-a), the load displacement curves of all four different FE-meshes show practically the same post-peak path. In Fig. (17-b) it can also be observed the load-displacement curves obtained with the local model when considering both regular meshes (coarse and fine). Contrarily to the results with the proposed non-local constitutive theory, the post-peak behaviors of the local model show relevant loss of objectivity regarding FE-element size.

8. Conclusions

In this work a thermodynamically consistent elastoplastic gradient-based constitutive theory for porous materials like concrete is proposed to predict its failure behavior when subjected to combined thermo-mechanical effects, including very high temperature fields. The maximum strength criterion is based on a combination between the Drucker-Prager and Modified Leon criteria as defined by Vrech and Etse (2009), which was extended in this work to include the strength degradation due to temperature effect. In the post-peak regime the material strength is composed by two mechanisms in parallel. One based on fracture-energy concepts, while the other on the gradient theory. Both strength contributions are temperature dependent through their corresponding characteristic length definitions, which also take into account the confinement pressure effect on the overall mechanical behavior. The pre-peak regime is defined through a local, isotropic, as well as temperature- and confinement-dependent, hardening rule. The numerical results included in this work demonstrate the predictive capabilities of the proposed constitutive theory for failure behaviors of concrete affected by temperature and subjected to stress histories in both compressive and tensile regimes. The results demonstrate also the combined effects of confinement pressure and temperature on the failure behavior of concrete in the triaxial compressive regime, and the regularization capabilities of the temperature dependent failure patterns and post-peak branches provided by the proposed non-local poroplastic theory.

9. Acknowledgements

The authors acknowledge the financial support for this work by CONICET (National Council of Scientific and Technical Research, Argentina) through the Grant No. PIP 112-2011010-1079 by CIUNT (Research Council of the University of Tucumán, Argentina) trhough the Grant No. 26/E479 and UBA (University of Buenos Aires, Argentina) through the Grant No. 20020090100 139.

References

Abu Al-Rub, R.K., Darabi, M.K., 2012. A thermodynamic framework for constitutive modeling of time- and rate-dependent materials. Part i: Theory. Int. J. Plasticity 34, 61–92.

Aifantis, E.C., 1984. On the microestructural origin of certain inelastic models. J. Eng. Mater. Technol. 106, 326–330.

Aifantis, E.C., 1987. The physics of plastic deformation. Int. J. Plasticity 3, 211–247.

Aifantis, E.C., Zbib, H.M., 1988. On the localization and postlocalization behaviour of plastic deformation. III, Res. Mechanica. 23, 261–305.

Anderberg, Y., Thelandersson, S., 1976. Stress and deformation characteristics of concrete at high temperatures: 2. Experimental investigation and material behavior mode., in: Bulletin 54, Lund Institute of Technology, Luden, Sweden., pp. 1–85.

Baker, G., 1996. The effect of exposure to elevated temperatures on the fracture energy of plain concrete. Mater. Struct. 39, 47–61.

Balendran, R.V., Nadeem, A., Maqsood, T., Leung, H.Y., 2003. Flexural and split cylinder strengths of HSC at elevated temperatures. Fire Technol. 29, 383–388.

Bazant, Z.P., Oh, B., 1983. Crack band theory for fracture concrete. Mater. Struct. 16, 155–177.

Belytschko, T., Lasry, D., 1989. A study of localization limiters for strain-softening in statics and dynamics. Comp. and Struct. 33, 707–715.

Bonelli, S., Millet, O., Nicot, J., Rahmoun, J., De Saxcé, G., 2012. On the definition of an average strain tensor for two-dimensional granular material assemblies. Int. J. Solids Struct. 49, 947–958.

de Borst, R., 1991. Simulation of strain localization: A reappraisal of the Cosserat continuum. Eng. Comp. 8, 317–332.

Canadija, M., Brnic, J., 2004. Associative coupled thermoplasticity at finite strain with temperature-dependent material parameters. Int. J. Plasticity. 20, 1851–1874.

Castillo, C., Durrani, A.J., 1990. Effect of transient high temperature on high-strength concrete. ACI Mater. J. 87, 47–53.

Chan, Y.N., Peng, G.F., Anson, M., 1999. Residual strength and pore structure of high-strength concrete and normal strength concrete after exposure to high temperatures. Cement Concrete Comp. 21, 23–27.
Chan, Y.N., Peng, G.F., Chan, J.K.W., 1996. Comparison between high strength concrete and normal strength concrete subjected to high temperature. Mater. Struct. 29, 616–619.
Chang, Y.F., Chen, Y.H., Sheu, M.S., Yao, G.C., 2006. Residual stress-strain relationship for concrete after exposure to high temperatures. Cement Concrete Res. 36, 1999–2005.
Chung, J., Consolazio, G., 2005. Numerical modeling of transport phenomena in reinforced concrete exposed to elevated temperatures. Cement. Concrete Res. 35, 597–608.
Coleman, B.D., Hodgdon, M.L., 1985. On shear bands in ductile materials. Arch. Rat. Mech. Anal. 90, 219–247.
Coussy, O., 1995. Mechanics of Porous Continua. John Wiley & Sons.
Coussy, O., 2004. Poromechanics. John Wiley & Sons.
Dal Pont, S., Ehrlacher, A., 2004. Numerical and experimental analysis of chemical dehydration, heat and mass transfers in a concrete hollow cylinder submitted to high temperatures. Int. J. Heat Mass Tran. 47, 135–147.
De Morais, M., Pliya, P., Noumow, A., Beaucour, A., Ortola, S., 2010. Numerical and experimental analysis of chemical dehydration, heat and mass transfers in a concrete hollow cylinder submitted to high temperatures. Nucl. Eng. Des. 240, 2655–63.
Della Croce, G., Giaccio, G., Villa, I., Zerbino, R., 2000. Resistencia y deformabilidad en compresión de hormigones afectados por altas temperaturas, in: Jornadas SAM 2000 - IV Coloquio Latinoamericano de Fractura y Fatiga, pp. 1151–1157.
Diederichs, U., Jumppanen, U.M., Penttala, V., 1988. Material properties of high strength concrete at elevated temperature, in: IABSE Thirteenth Congress, Helsinki, Finland, pp. 151–181.
Dietsche, A., Steinmann, P., Willam, K., 1993. Micropolar elastoplasticity and its role in localization. Int. J. Plast.. 7, 813–831.
Etse, G., Steinmann, P., Nieto, M., 2003. A micropolar microplane theory. Int. Journal of Engineering Sciences. 41, 1631–48.
Etse, G., Steinmann, P., Willam, K., 1991. Computational aspects of localized failure simulations in plain concrete. Int. RILEM/ESIS Publication on Fracture Processes in Concrete, Rock and Ceramics. 2, 651–660.
Etse, G., Willam, K., 1994. Fracture energy formulation for inelastic behavior of plain concrete. J. Eng. Mech. 120, 1983–2011.
Feraille-Fresnet, A., Tamagny, P., Ehrlacher, A., Sercombe, J., 2003. Thermo-hydro-chemical modelling of a porous medium submitted to high temperature: An application to an axisymmetrical structure. Math. Comput. Model. 37, 641–650.
Forest, S., Aifantis, E.C., 2010. Some links between recent gradient thermo-elasto-plasticity theories and the thermomechanics of generalized continua. Int. J. Solids Struct. 47, 3367–76.
Gawin, D., Majorana, C.E., Pesavento, F., Schrefler, B.A., 1998. A fully coupled multiphase finite element model of hygro-thermo-mechanical behaviour of concrete at high temperature, in: Computational Mechanics New Trends and Applications, CIMNE, Barcelona, Spain.
Gawin, D., Pesavento, F., Schrefler, B.A., 2003. Modelling of hygro-thermal behaviour of concrete at high temperature with thermo-chemical and mechanical material degradation. Comput. Method Appl. M. 192, 1731–1771.
Gawin, D., Pesavento, F., Schrefler, B.A., 2004. Modelling of deformations of high strength concrete at elevated temperatures. Mater. Struct. 37, 218–236.
Gawin, D., Pesavento, F., Schrefler, B.A., 2006. Towards prediction of the thermal spalling risk through a multi-phase porous media model of concrete. Comput. Method Appl. M. 195, 5707–5729.
Hurlbut, B., 1985. Experimental and computational investigation of strain-softening in concrete. Master Thesis.. University of Colorado.
Janotka, I., Bagel, L., 2002. Pore structures, permeabilities, and compressive strengths of concrete at temperatures up to 800°C. ACI Mater. J. 100, 196–200.
Jiang, T., Shao, J.F., 2012. Micromechanical analysis of the nonlinear behavior of porous geomaterials based on the fast fourier transform. Comput. Geotech. 46, 69–74.
Jooss, M., Reinhardt, H.W., 2002. Permeability and diffusivity of concrete as function of temperature. Cement. Concrete Res. 32, 1497–1504.
Kamrin, K., 2010. Nonlinear elasto-plastic model for dense granular flow. Int. J. Plasticity 26, 167–188.
Khennane, A., Baker, G., 1992a. Plasticity models for the biaxial behaviour of concrete at elevated temperatures. Part I: Failure criterion. Comput. Method Appl. M. 100, 207–223.
Khennane, A., Baker, G., 1992b. Plasticity models for the biaxial behaviour of concrete at elevated temperatures. Part II: Implementation and simulation tests. Comput. Method Appl. M. 100, 225–248.
La Ragione, L., Prantil, V.C., Sharma, I., 2008. A simplified model for inelastic behavior of an idealized granular material. Int. J. Plasticity 24, 168–189.
Lee, J., Xi, Y., Willam, K., 2008. Properties of concrete after high-temperature heating and cooling. ACI Mater. J. 105, 334–341.
Leon, A., 1935. Ueber das Mass der Anstrenung bei Beton. Ingenieur Archiv 4, 421–431.
Li, M., Qian, C., Sun, W., 2004. Mechanical properties of high-strength concrete after fire. Cement. Concrete Res. 34, 1001–05.
Loeffel, K., Anand, L., 2011. A chemo-thermo-mechanically coupled theory for elasticviscoplastic deformation, diffusion, and volumetric swelling due to a chemical reaction. Int. J. Plasticity 27, 1409–1431.
Majumdar, P., Gupta, A., Marchetas, A., 1995. Moistures propagation and resulting stress in heated concrete walls. Nucl. Eng. Des. 156, 147–158.
Martinelli, E., Koenders, E., Caggiano, A., 2013. A numerical recipe for modelling hydration and heat flow in hardening concrete. Cement Concrete Comp. 40, 48–58.
Mehmet, S.C., Ozturan, T., 2010. Mechanical properties of normal and high strength concretes subjected to high temperatures and using image analysis to detect bond deteriorations. Constr. Build. Mater. 24, 1486–93.
Menou, A., Mounajed, G., Boussa, H., Pineaud, A., Carre, H., 2006. Residual fracture energy of cement paste, mortar and concrete subject to high temperature. Theor. Appl. Fract. Mec. 45, 64–71.
Mihashi, H., Numao, T., Fukuzawa, K., 1992. Simultaneous heat and mass transfer in heated concrete, in: 3rd International Workshop: Behaviour of Concrete Elements under Thermal and Hygral Gradients. Weimar, Germany.
Mindeguia, J.C., Pimienta, P., Noumow, A., Kanema, M., 2010. Temperature, pore pressure and mass variation of concrete subjected to high temperature experimental and numerical discussion on spalling risk. Cement. Concrete Res. 40, 477–487.

Mroginski, J., Etse, G., 2013. A finite element formulation of gradient-based plasticity for porous media with C_1 interpolation of state variables. Comput. Geotech. 49, 7–17.
Mroginski, J., Etse, G., 2014. Discontinuous bifurcation analysis in thermodynamically consistent gradient poroplastic materials. Int. J. Solids Struct. 51, 1834–1846.
Mroginski, J., Etse, G., Vrech, S., 2011. A thermodynamical gradient theory for deformation and strain localization of porous media. Int. J. Plasticity. 27, 620–634.
Muehlhaus, H.B., Vardoulakis, I., 1987. The thickness of shear bands in granular materials. Geotechnique 37, 271–283.
Muraleetharan, K.K., Liu, C., Wei, C., Kibbey, T.C.G., Chen, L., 2009. An elastoplatic framework for coupling hydraulic and mechanical behavior of unsaturated soils. Int. J. Plasticity 25, 473–490.
Nicot, F., Darve, F., 2007. A micro-mechanical investigation of bifurcation in granular materials. Int. J. Solids Struct. 44, 6630–6652.
Nicot, F., Hadda, N., Guessasma, M., Fortin, J., Millet, O., 2013. On the definition of the stress tensor in granular media. Int. J. Solids Struct. 50, 2508–2517.
Nicot, F., Sibille, L., Darve, F., 2009. Bifurcation in granular materials: An attempt for a unified framework. Int. J. Solids Struct. 46, 3938–3947.
Nicot, F., Sibille, L., Darve, F., 2012. Failure in rate-independent granular materials as a bifurcation toward a dynamic regime. Int. J. Plasticity 29, 136–154.
Nielsen, C.V., Bicanic, N., 2003. Residual fracture energy of high-performance and normal concrete subject to high temperatures. Mater. Struct. 36, 545–521.
Obeid, W., G., Alliche, A., Mounajed, G., 2001. Identification of the physical parameters used in the thermo-hygro-mechanical model. Transport Porous Med. 45, 215–239.
Obeid, W., Mounajed, G., Alliche, A., 2011. Mathematical formulation of thermo-hygro-mechanical coupling problem in non-saturated porous media. Comput. Method Appl. M. 190, 5105–5122.
Ortiz, M., 1985. A constitutive theory for the inelastic behaviour of concrete. Mech. Mater. 4, 67–93.
Pan, Z., Sanjayan, J.G., Kong, D.L.Y., 2012. Effect of aggregate size on spalling of geopolymer and portland cement concretes subjected to elevated temperatures. Constr. Build. Mater. 36, 365–372.
Prato, T., Cervera, M., Oliver, J., 1997. Simulación numérica del proceso de hidratación del hormigón. CIMNE N 114, Barcelona .
Sercombe, J., Ulm, F.J., Mang, H.A., 1998. Consistent return mapping algorithm for chemoplastic constitutive laws with internal couplings. Int. J. Numer. Meth. Eng. 47, 75–100.
Shen, W.Q., Kondo, D., Dormieux, L., Shao, J.F., 2013. A closed-form three scale model for ductile rocks with a plastically compressible porous matrix. Mech. Mater. 59, 73–86.
Shen, W.Q., Shao, J.F., Kondo, D., Gatmiri, B., 2012. A micromacro model for clayey rocks with a plastic compressible porous matrix. Int. J. Plasticity 36, 64–85.
Shojaei, A., Dahi Taleghani, A., Li, G., 2014. A continuum damage failure model for hydraulic fracturing of porous rocks. Int. J. Plasticity. 59, 199–212.
Shojaei, A., Voyiadjis, G.Z., Tan, P.J., 2013. Viscoplastic constitutive theory for brittle to ductile damage in polycrystalline materials under dynamic loading. Int. J. Plasticity. 48, 125–151.
Simo, J., Miehe, C., 1992. Associative coupled thermoplasticity at finite strains: formulation, numerical analysis and implementation. Comput. Method Appl. M. 98, 41–104.
Sluys, L.J., de Borst, R., 1991. Solutions methods for localization in fracture dynamics, in: Conf. on fracture in concrete, Rock and Ceramics, pp. 661–671.
Svedberg, T., 1999. On the modelling and numerics of gradient-regularized plasticity coupled to damage. PhD. Thesis. Chalmers University of Technology. Goteborg, Sweden.
Svedberg, T., Runesson, K., 1997. A thermodynamically consistent theory of gradient-regularized plasticity coupled to damage. Int. J. Plasticity. 13, 669–696.
Tenchev, R., Li, L., Purkiss, J., 2001. Finite element analysis of coupled heat and moisture transfer in concrete subjected to fire. Numer. Heat Tr. A-Appl. 39, 685–710.
Tenchev, R., Li, L., Purkiss, J., 2005. An application of a damage constitutive model to concrete at high temperature and prediction of spalling. Int. J. Solids Struct. 42, 655065.
Tran, T.H., Monchiet, V., Bonnet, G., 2012. A micromechanics-based approach for the derivation of constitutive elastic coefficients of strain-gradient media. Int. J. Solids Struct. 49, 783–792.
Ulm, F.J., Coussy, O., 1995. Modeling of thermochemomechanical couplings of concrete at early ages. J. Eng. Mech. ASCE. 121, 785–794.
Ulm, F.J., Coussy, O., 1996. Strength growth as chemoplastic hardening in early age concrete. J. Eng. Mech. ASCE. 122, 1123–1132.
Ulm, F.J., Coussy, O., 1999. The chunnel fire I: Chemoplastic softening in rapidly heated concrete. J. Eng. Mech.-ASCE. 125, 272–289.
Vardoulakis, I., Aifantis, E.C., 1991. A gradient flow theory of plasticity for granular materials. Acta Mechanica. 87, 197–217.
Voyiadjis, G.Z., Faghihi, D., 2012. Thermo-mechanical strain gradient plasticity with energetic and dissipative length scales. Int. J. Plasticity 31, 218–247.
Voyiadjis, G.Z., Shojaei, A., Li, G., 2011. A thermodynamic consistent damage and healing model for self healing materials. Int. J. Plasticity 27, 1025–1044.
Voyiadjis, G.Z., Shojaei, A., Li, G., 2012a. A generalized coupled viscoplastic- viscodamage- viscohealing theory for glassy polymers. Int. J. Plasticity 28, 21–45.
Voyiadjis, G.Z., Shojaei, A., Li, G., Kattan, P.I., 2012b. A theory of anisotropic healing and damage mechanics of materials., in: Royal Society A: Mathematical, Physical and Engineering Science, pp. 163–183.
Vrech, S., Etse, G., 2007. FE approach for thermodynamically consistent gradient-dependent plasticity. Latin Am. Appl. Res. 37, 127–132.
Vrech, S., Etse, G., 2009. Gradient and fracture energy-based plasticity theory for quasi-brittle materials like concrete. Comput. Method Appl. M. 199, 136–147.
Willam, K., Etse, G., 1990. Failure assessment of the extended Leon model for plain concrete., in: SCI-C Conf., Zell and See, Austria, Pineridge

Press, Swansea, UK., pp. 851–870.
Willam, K., Hurbult, B., Sture, S., 1985. Experimental and constitutive aspects of concrete failure., in: US-Japan Seminar on Finite Element Analysis of Reinforced Concrete Structures., pp. 226–254.
Willam, K.J., Bicanic, N., Sture, S., 1984. Constitutive and computational aspects of strain-softening and localization in solids., in: Int. Conf. Computer Aided Analysis and Design of concrete Structures, Swansea., pp. 33–70.
Wippler, J., Funfschilling, S., Fritzen, F., Bohkle, T., Hoffmann, M., 2011. Homogenization of the thermoelastic properties of silicon nitride. Acta Mater. 59, 6029–6038.
Xie, N., Zhu, Q.Z., Hu, L.H., Shao, J.F., 2011. A micromechanics-based elastoplastic damage model for quasi-brittle rocks. Comput. Geotech. 38, 970–977.
Xie, S.Y., Sha, J.F., 2012. Experimental investigation and poroplastic modelling of saturated porous geomaterials. Int. J. Plasticity 39, 27–45.
Yin, Z., Chang, C.S., Hicher, P., Karstunen, M., 2009. Micromechanical analysis of kinematic hardening in natural clay. Int. J. Plasticity. 25, 1413–1435.
Zeim, M., Lackner, R., Leithner, D., Eberhardsteiner, J., 2008. Identification of residual gas-transport properties of concrete subjected to high temperatures. Cement. Concrete Res. 38, 699–716.
Zhang, B., 2011. Effects of moisture evaporation (weight loss) on fracture properties of high performance concrete subjected to high temperatures. Fire Safety J. 46, 543–549.
Zhang, B., Bicanic, N., 2002. Residual fracture toughness of normal- and high-strength gravel concrete after heating to 600°C. ACI Mater. J. 99, 217–226.
Zhang, S., leng, W., Zhang, F., Xiong, Y., 2012. A simple thermo-elastoplastic model for geomaterials. Int. J. Plasticity 34, 93–113.
Zhen-jun, H., Yu-pu, S., 2010. Multiaxial tensile-compressive strengths and failure criterion of plain high-performance concrete before and after high temperatures. Constr. Build. Mater. 24, 498–504.
Zhou, Y., Rajapakse, R., J., G., 1998. Coupled heat-moisture-air transfer in deformable unsaturated media. J. Eng. Mech.-ASCE 124, 1090–1099.
Zhu, Q.Z., Shao, J.F., Mainguy, M., 2010. A micromechanics-based elastoplastic damage model for granular materials at low confining pressure. Int. J. Plasticity. 26, 586–602.

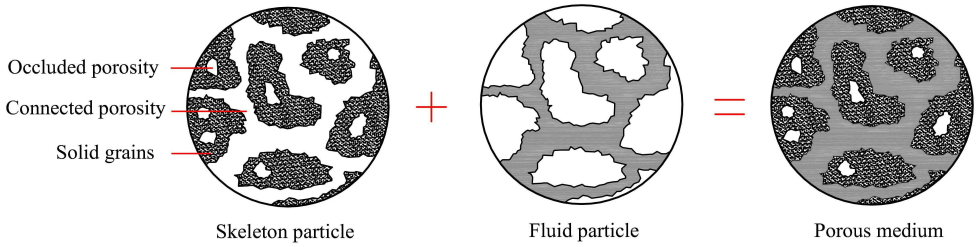

Figure 1: Porous medium composed by the superimposition (in space and time) of a skeleton particle and a fluid particle.

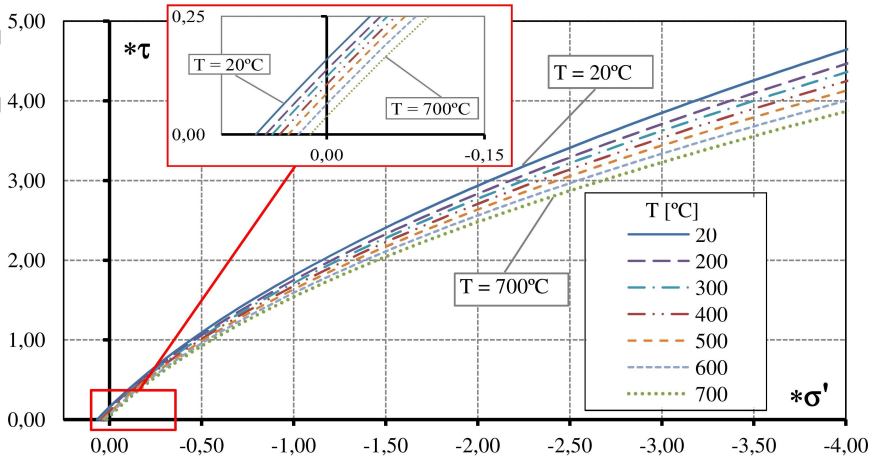

Figure 2: TD-LDP Failure surfaces in the compression meridian for variable temperature levels.

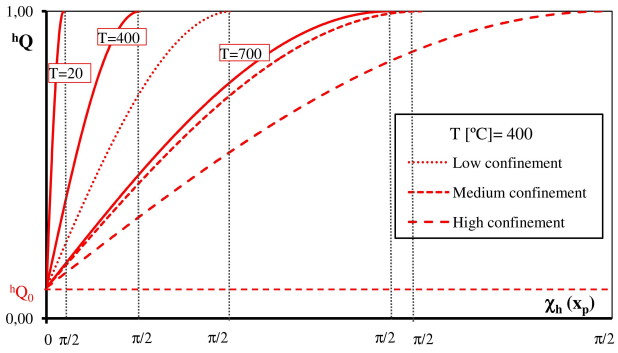

Figure 3: Evolution of hardening dissipative stress ${}^{h}Q$ with the hardening variable χ_h for different temperature levels (20°C, 400°C and 700°C) and different confinement levels at 400°C

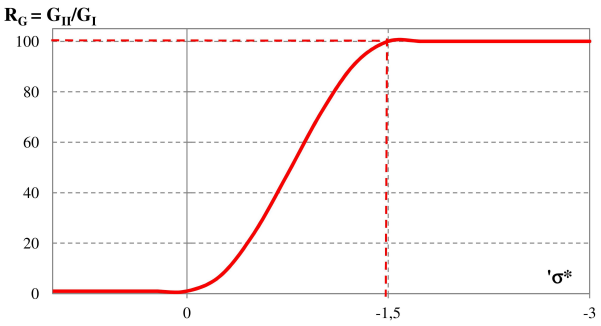

Figure 4: Variation of R_G with the confinement pressure.

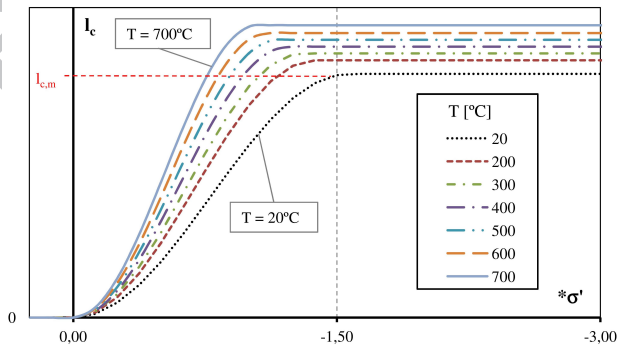

Figure 5: Variation of the gradient characteristic length l_c, in terms of both: temperature level and confinement pressure.

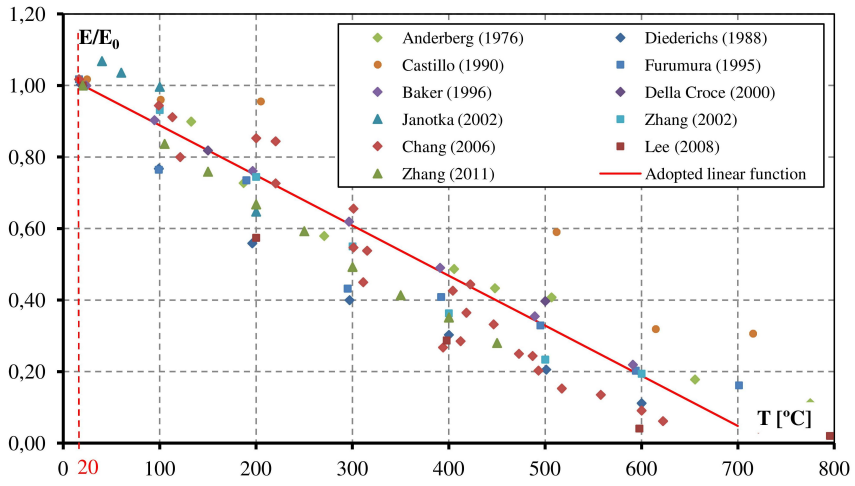

Figure 6: Approximated concrete elasticity modulus function, depending on the acting temperature and experimental data.

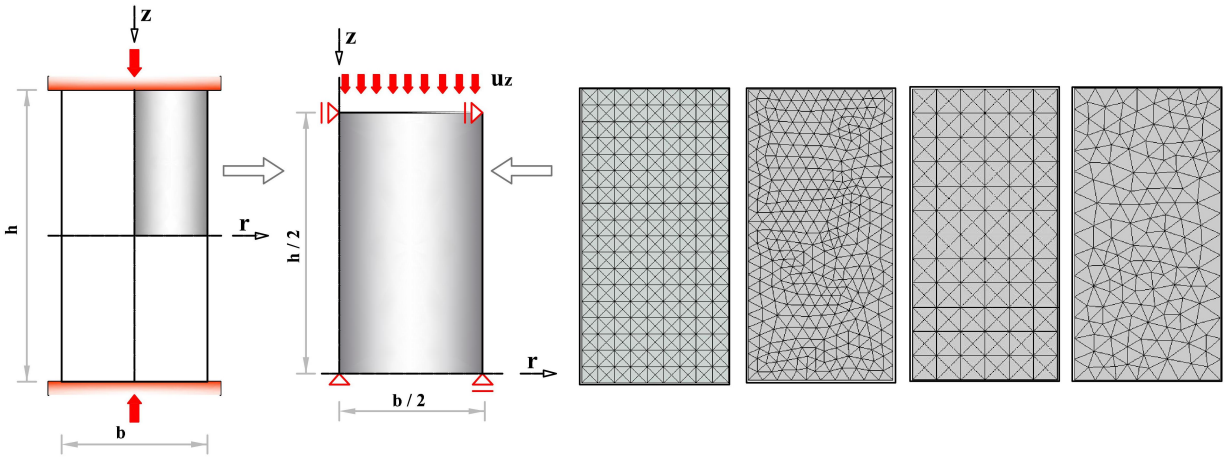

Figure 7: Axisymmetrical concrete cylinder, boundary conditions and FE mesh discretization.

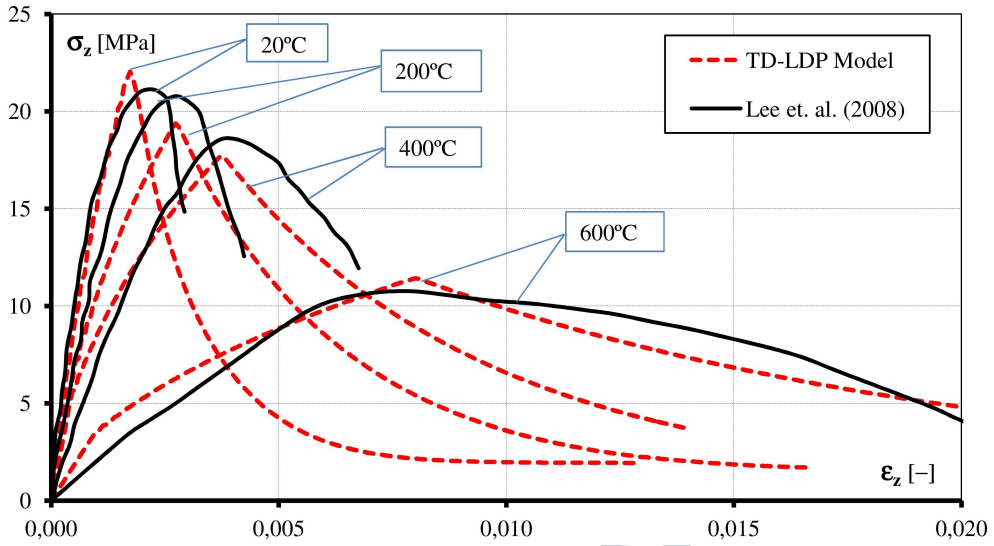

Figure 8: Numerical predictions of the TD-LDP model and experimental results by Lee et al. (2008) of uniaxial compression tests under increasing temperatures.

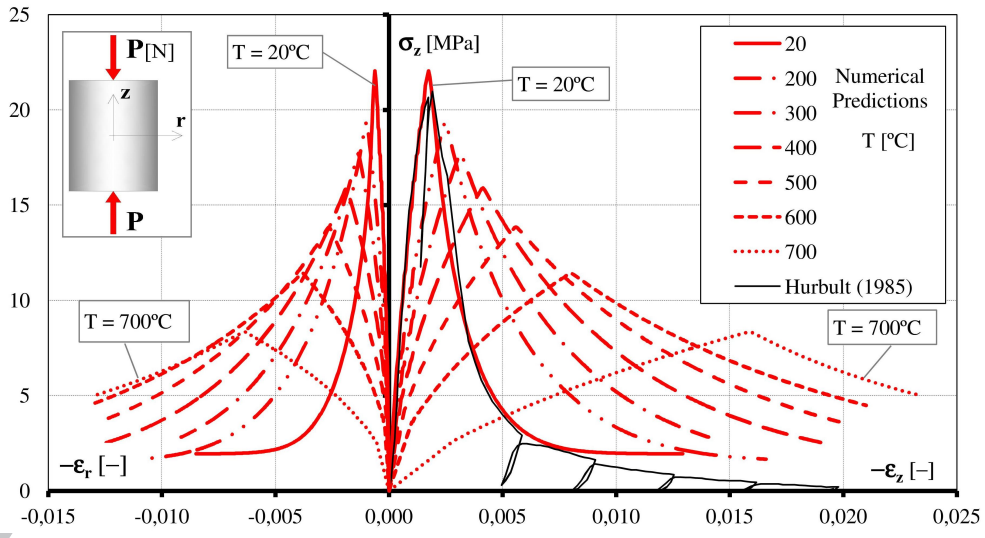

Figure 9: Numerical predictions of the TD-LDP model of uniaxial compression tests on concrete subjected to different temperature levels.

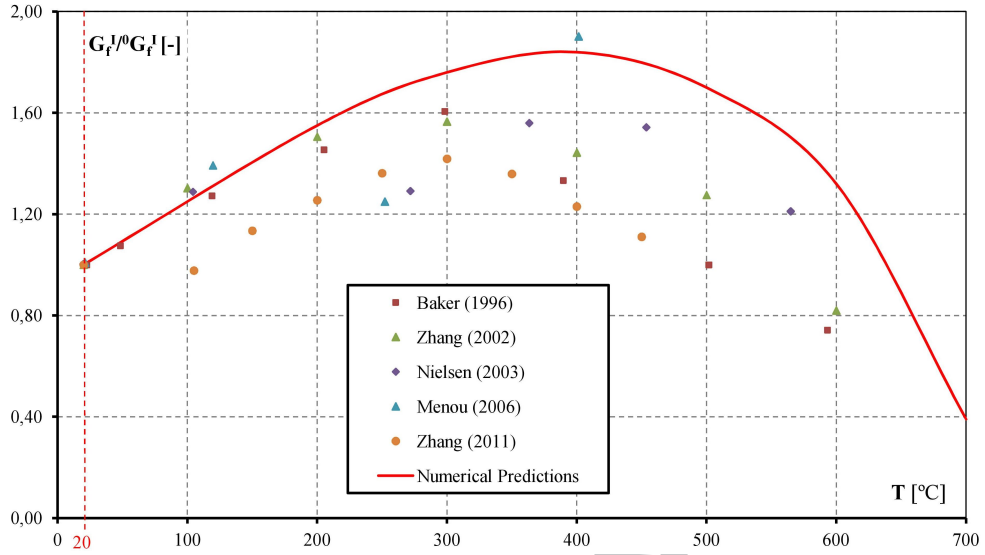

Figure 10: Variation of the normalized fracture energy released in uniaxial tensile tests performed at different temperature levels.

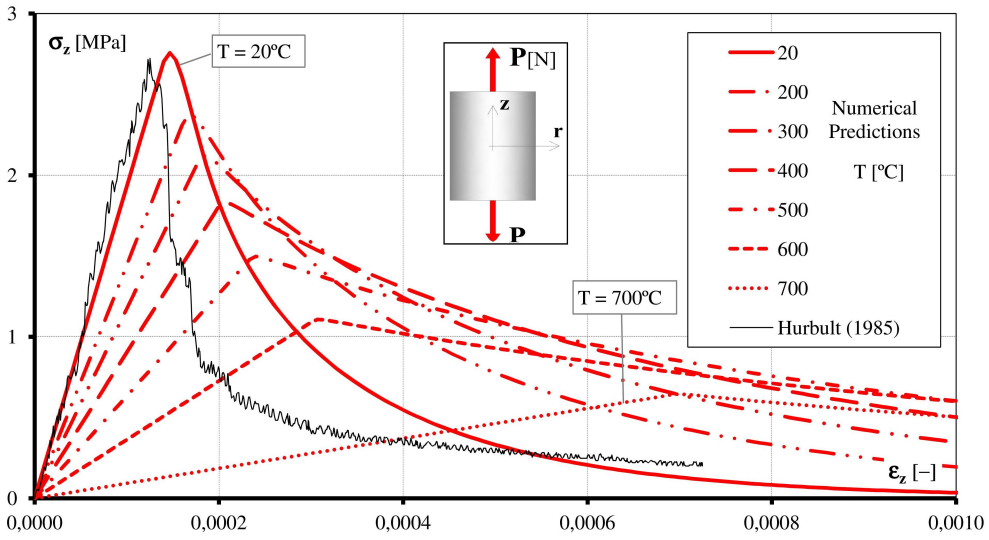

Figure 11: Numerical model predictions of uniaxial tensile tests on concrete cylindrical specimens under variable temperature levels.

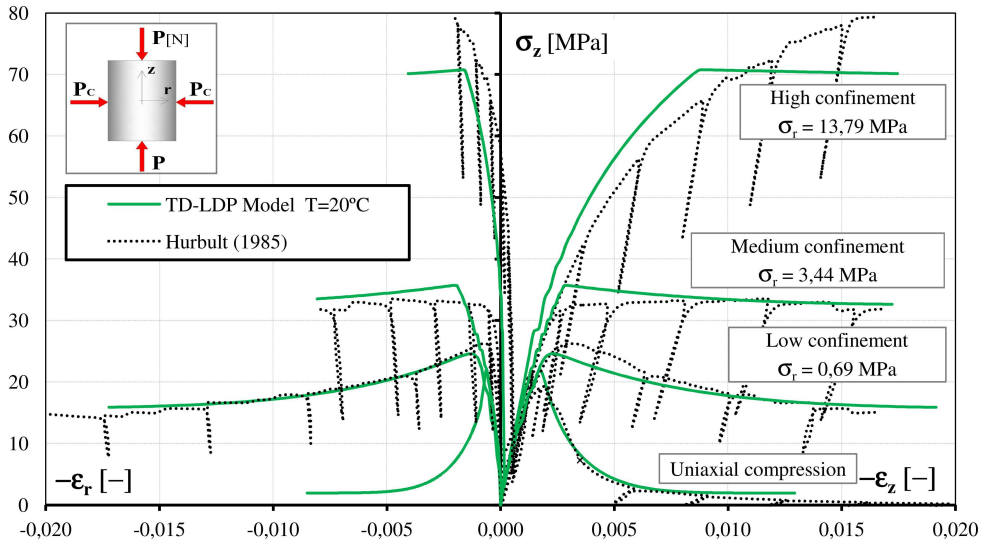

Figure 12: Numerical model predictions of triaxial tests on normal concrete at 20°C. Comparison with experimental results by Hurlbut (1985).

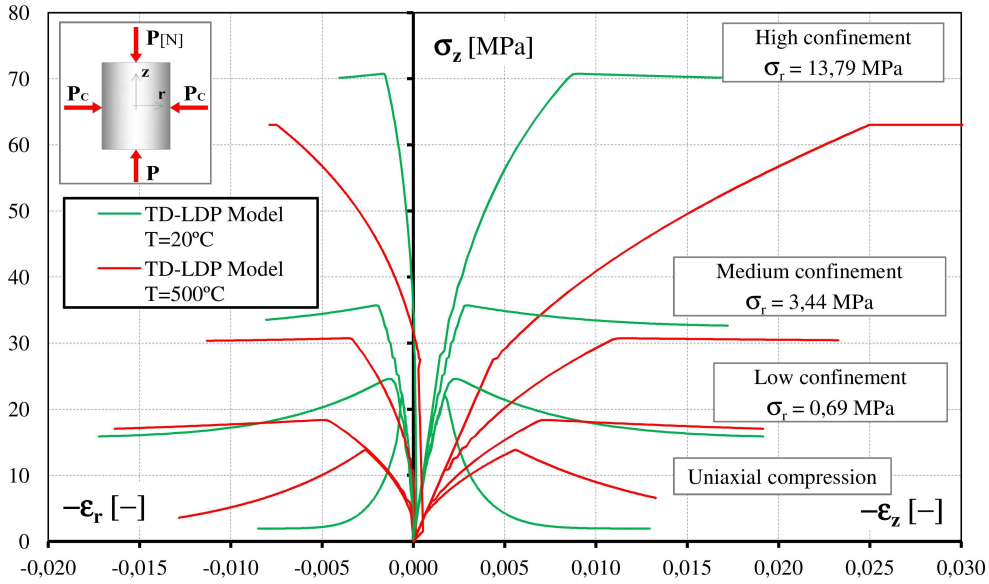

Figure 13: Numerical model predictions of triaxial compression tests on concrete cylinders at 500°C.

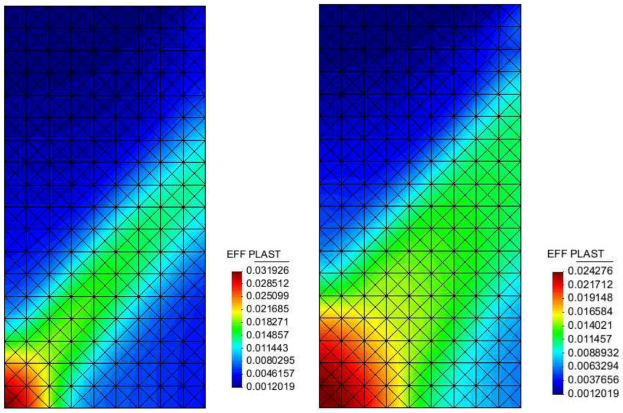

Figure 14: Equivalent plastic strain distribution at residual stress of the uniaxial compression test under: (a) 20°C and (b) 500°C.

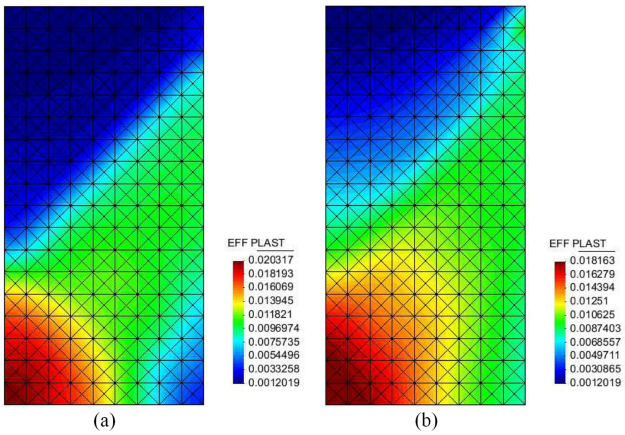

Figure 15: Equivalent plastic strain distribution at residual stress of the triaxial compression test with medium confinement (σ_r = 3.44MPa) under: (a) 20°C and (b) 500°C.

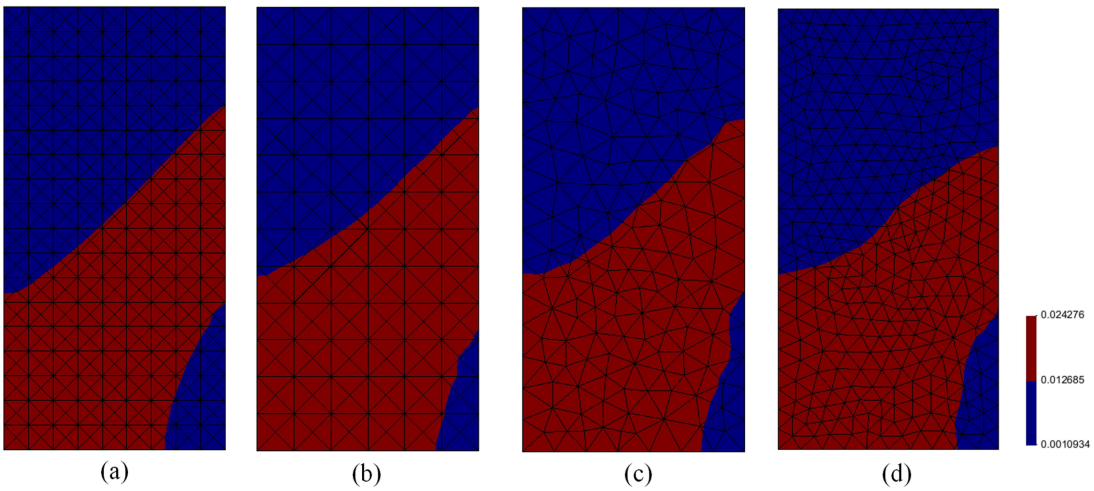

Figure 16: Equivalent plastic strain distribution obtained with the proposed model at residual stress of the uniaxial compression test under 500°C for 4 different FE discretizations.

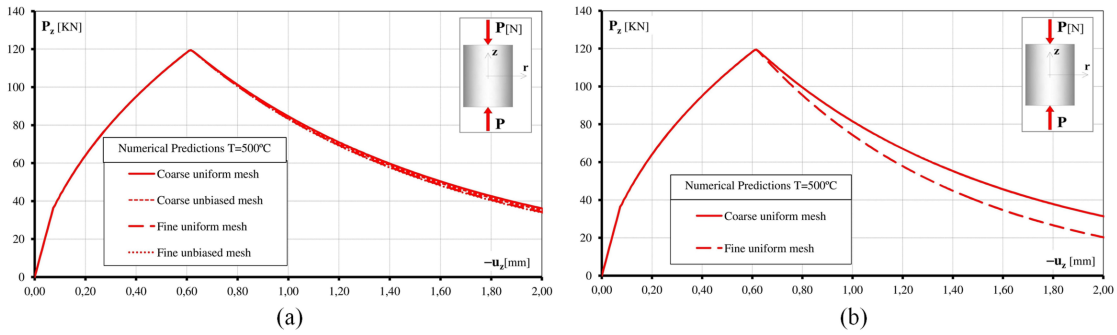

Figure 17: Load-displacement curves obtained with the: (a) non-local and (b) local model formulations.

Highlights

1. A thermodynamically consistent model for porous materials under high temperatures is proposed.

2. Non-local effects are considered in the post-peak regime.

3. Post-peak behaviour is divided into a fracture-energy and a gradient-theory based terms.

4. Combined effects of confinement pressure and high temperatures are analysed.

5. Regularization capabilities of the proposed non-local model are demonstrated.